Supporting Information

Receptor-Specific Molecular Recognition of Maresin 1 and Docosahexaenoic Acid by the Nuclear Receptors PPARα, PPARγ, and RORα

Matías Quiñones San Martín [1,2], Christian Olivera-Fuentes [2,3], Francisca Herrera-Vielma [1], Ramón Norambuena-González [1,4], Eduardo Solís-Céspedes [5], Daniel R. González [1], Yunier Perera-Sardiña [1,*] and Jessica Zúñiga-Hernández [1,*]

[1] Laboratory of Pharmacology and Physiology, Department of Basic Biomedical Sciences, Faculty of Health Sciences, University of Talca, Talca 3460000, Chile; mquinones@utalca.cl (M.Q.S.M.); f.herrera.vielma@gmail.com (F.H.-V.); ramon.norambuena@utalca.cl (R.N.-G.); dagonzalez@utalca.cl (D.R.G.)
[2] Doctorate in Science Program, mention in Research and Development of Bioactive Products, Institute of Chemistry of Natural Resources, University of Talca, Talca 3460000, Chile; colivera15@alumnos.utalca.cl
[3] Laboratory of Molecular Physiology, Faculty of Medicine, University of Talca, Talca 3460000, Chile
[4] Doctorate in Biomedical Sciences Program, Faculty of Health Sciences, University of Talca, Talca 3460000, Chile
[5] Department of Preclinical Sciences, Faculty of Medicine, Catholic University of Maule, Talca 3460000, Chile; esolis@ucm.cl
* Correspondence: yunier.perera@utalca.cl (Y.P.-S.); jezuniga@utalca.cl (J.Z.-H.)

This Supporting Information is organized into two sections: Supplementary Tables (Tables S1–S12) and Supplementary Figures (Figures S1–S8). Within each section, the items are arranged according to the order in which the corresponding analyses are presented in the main manuscript. Tables S9 and S10 provide the audited ligand oxygen-atom assignments and the replica-level distance values underlying Figure 3, respectively. Detailed computational procedures are provided in Sections 2.1–2.10 of the main manuscript; therefore, no separate Extended Methods section is included here.

Abbreviations and conventions.

HB, hydrogen bond; HIE, neutral histidine protonated at Nε2; WB, water bridge; AF-2, activation function-2; H12, helix 12; LBD, ligand-binding domain; MD, molecular dynamics; RMSD, root-mean-square deviation; RMSF, root-mean-square fluctuation; Rg, radius of gyration; FEL, free-energy landscape; PCA, principal component analysis; MM-GBSA, molecular mechanics/generalized Born surface area.

Unit convention. FEL RMSD–Rg coordinates and Rg profiles are reported in nm, whereas redocking and ligand heavy-atom RMSD, protein Cα RMSD/RMSF, and residue–ligand distances are reported in Å (1 nm = 10 Å).

1. Supplementary Tables

Table S1. Crystallographic structures screened for receptor-template selection and structural comparison

Receptor	PDB	Selection status	Rationale	Resolution (Å)	R-work	R-free	Ligand(s)	Mutations	Year
PPARα	2P54	Selected as docking template	High-resolution wild-type PPARα holo structure with a resolved pocket, AF-2/H12 region, reference ligand, and SRC1 peptide; provides an independent non-fatty-acid template.	1.79	0.204	0.227	735	none	2007
PPARα	1KKQ	Not selected	Lower resolution and less favorable overall validation metrics than 2P54.	3.00	0.258	0.290	471	none	2002
PPARα	1K7L	Not selected	Lower resolution and less favorable overall validation metrics than 2P54.	2.50	0.247	0.284	544, YT3	none	2001
PPARα	6LX7	Retained as comparative structural reference	High-resolution endogenous fatty-acid-bound structure; not used as the primary template to avoid preferential bias toward a fatty-acid binding mode.	1.41	0.175	0.192	STE, GOL	none	2020
PPARα	6LX8	Retained as comparative structural reference	High-resolution endogenous fatty-acid-bound structure; retained to document a chemically related pocket conformation.	1.54	0.180	0.198	OLA, GOL	none	2020
PPARα	7BQ1	Retained as comparative structural reference	High-resolution endogenous fatty-acid-bound structure; retained as a structurally relevant lipid-bound comparator.	1.52	0.194	0.213	PLM, GOL	none	2020
PPARγ	6MS7	Selected as docking template	Highest-resolution screened PPARγ holo structure with a resolved AF-2/H12 region, reference ligand, and coactivator peptide.	1.43	0.186	0.208	V77	none	2019

Receptor	PDB	Selection status	Rationale	Resolution (Å)	R-work	R-free	Ligand(s)	Mutations	Year
PPARγ	2VV0	Retained as comparative structural reference	DHA-bound PPARγ structure; highly relevant chemically but lower in resolution and potentially biased toward DHA.	2.55	0.218	0.261	HXA	none	2008
PPARγ	2VV1	Retained as comparative structural reference	PPARγ structures containing related oxidized fatty acids; used to contextualize alternative lipid-binding arrangements but not as primary templates.	2.20	0.239	0.277	4HD	none	2008
PPARγ	2VV3	Retained as comparative structural reference	PPARγ structures containing related oxidized fatty acids; used to contextualize alternative lipid-binding arrangements but not as primary templates.	2.85	0.225	0.252	4R8	none	2008
PPARγ	2VSR	Retained as comparative structural reference	PPARγ structures containing related oxidized fatty acids; used to contextualize alternative lipid-binding arrangements but not as primary templates.	2.05	0.226	0.266	9HO	none	2008
PPARγ	2VST	Retained as comparative structural reference	PPARγ structures containing related oxidized fatty acids; used to contextualize alternative lipid-binding arrangements but not as primary templates.	2.35	0.234	0.274	243	none	2008
PPARγ	2VV2	Retained as comparative structural reference	PPARγ structures containing related oxidized fatty acids; used to contextualize alternative lipid-binding arrangements but not as primary templates.	2.75	0.223	0.263	5HE	none	2008
PPARγ	2VV4	Retained as comparative structural reference	PPARγ structures containing related oxidized fatty acids; used to contextualize alternative lipid-binding	2.35	0.226	0.252	6OC, 6OB	none	2008

Receptor	PDB	Selection status	Rationale	Resolution (Å)	R-work	R-free	Ligand(s)	Mutations	Year
			arrangements but not as primary templates.						
PPARγ	2PRG	Not selected	Classical agonist-bound reference with lower resolution than 6MS7 and less suitable for the independent-template strategy.	2.30	0.207	0.264	BRL	none	1999
RORα	1N83	Selected as docking template	Highest-resolution screened wild-type RORα holo structure with a resolved cholesterol-bound sterol pocket.	1.63	0.201	0.223	CLR	none	2002
RORα	1S0X	Retained as comparative structural reference	Cholesterol-sulfate-bound RORα structure illustrating polarity-dependent repositioning, but with lower resolution than 1N83.	2.20	0.197	0.209	C3S	none	2004

Note: *Structures were identified by UniProt accession and screened among available X-ray structures of the human ligand-binding domain of each receptor. Entries containing receptor mutations, structures with a crystallographic resolution worse than 3.0 Å, and structures not corresponding to the ligand-binding domain were excluded during the initial filtering step. Primary docking templates were selected according to structural resolution and validation quality, completeness of the ligand-bound pocket and AF-2/H12 region, availability of an experimentally resolved ligand pose suitable for redocking, and use of an independent holo template that did not preferentially favor either MaR1 or DHA. Chemically related fatty-acid- and sterol-bound structures were retained as comparative structural references but were not used as primary docking templates.*

Table S2. wwPDB model- and ligand-validation metrics for the crystallographic structures included in the receptor-template screening.

Receptor	PDB	Resolution (Å)	R-free	Clashscore	Ramachandran outliers (%)	Rotamer outliers (%)	RSRZ outliers (%)	Ligand RSCC	Ligand RSR
PPARα	2P54	1.79	0.227	8.48	0.00	0.84	8.96	0.966	0.054
PPARα	1KKQ	3.00	0.290	52.11	6.34	20.10	—	—	—

Receptor	PDB	Resolution (Å)	R-free	Clashscore	Ramachandran outliers (%)	Rotamer outliers (%)	RSRZ outliers (%)	Ligand RSCC	Ligand RSR
PPARα	1K7L	2.50	0.284	38.12	4.08	11.94	—	—	—
PPARα	6LX7	1.41	0.192	3.26	0.00	0.85	4.10	—	—
PPARα	6LX8	1.54	0.198	3.57	0.00	0.43	3.41	—	—
PPARα	7BQ1	1.52	0.213	5.29	0.00	0.83	10.33	—	—
PPARγ	6MS7	1.43	0.208	4.87	0.00	0.40	14.86	0.854, 0.839	0.151, 0.144
PPARγ	2VV1	2.20	0.277	15.60	0.21	4.30	13.13	—	—
PPARγ	2VV3	2.85	0.252	17.13	0.61	7.57	3.58	—	—
PPARγ	2VSR	2.05	0.266	16.95	0.40	3.28	12.50	—	—
PPARγ	2VST	2.35	0.274	11.38	0.61	4.42	10.43	—	—
PPARγ	2VV2	2.75	0.263	19.15	0.20	6.75	3.51	—	—
PPARγ	2VV4	2.35	0.252	14.03	0.00	4.92	11.78	—	—
PPARγ	2PRG	2.30	0.264	21.01	1.91	1.21	—	—	—
PPARγ	2VV0	2.55	0.261	22.03	0.20	—	3.91	0.751, 0.842	0.318, 0.224
RORα	1N83	1.63	0.223	9.02	0.00	1.32	7.17	0.961	0.049
RORα	1S0X	2.20	0.209	9.49	0.80	1.75	1.59	—	—

Note: *Metrics were extracted from the corresponding wwPDB validation reports. A dash indicates that the metric was not reported in the validation file. When more than one crystallographic copy of a ligand was present, the corresponding ligand RSCC and RSR values are reported as comma-separated values in the same order in both columns.*

Table S3. Protein preparation, Glide grid generation, ligand preparation, hierarchical SP–XP docking, and redocking-validation parameters used for PPARα, PPARγ, and RORα.

Parameter	PPARα (2P54)	PPARγ (6MS7)	RORα (1N83)
Grid generation (Glide)			
Crystallographic resolution (Å)	1.79	1.43	1.63
Grid center (x, y, z) / Å	13.246, 39.546, 27.603	14.091, 34.948, 24.992	22.745, 25.044, 17.561
Centering reference	Co-crystallized ligand 735	Co-crystallized ligand V77	Co-crystallized cholesterol (CLR)
Inner box dimensions (Å)	10 × 10 × 10	10 × 10 × 10	10 × 10 × 10
Outer box dimensions (Å)	28.042 × 28.042 × 28.042	23.389 × 23.389 × 23.389	28.047 × 28.047 × 28.047
VdW radii scaling (grid generation)	1.00 (default)	1.00 (default)	1.00 (default)
Charge cutoff for polarity	0.250	0.250	0.250
Receptor polar sites (nsites)	125	125	125
Grid spacing / Å	1.0	1.0	1.0
Post-grid dimensions (nx, ny, nz)	80 × 80 × 80	64 × 64 × 64	72 × 72 × 80
Receptor preparation			
Protein Preparation Wizard	Applied	Applied	Applied
Schrödinger version	2020-3	2020-3	2020-3
Bond orders assigned	Yes	Yes	Yes
Hydrogens added	Yes	Yes	Yes
Protonation prediction	Epik (pH 7.4)	Epik (pH 7.4)	Epik (pH 7.4)
Force field	OPLS3e	OPLS3e	OPLS3e
Missing loops/side chains	Prime-modeled	Prime-modeled	Prime-modeled
Restrained minimization	impref, heavy-atom RMSD ≤ 0.30 Å	impref, heavy-atom RMSD ≤ 0.30 Å	impref, heavy-atom RMSD ≤ 0.30 Å

Parameter	PPARα (2P54)	PPARγ (6MS7)	RORα (1N83)
Waters removed beyond 5 Å from hetero groups	Yes	Yes	Yes
Ligand preparation (LigPrep)			
Force field	OPLS3e	OPLS3e	OPLS3e
Protonation	Epik (pH 7.4)	Epik (pH 7.4)	Epik (pH 7.4)
Stereocenter handling	ConfGen (biologically-relevant states retained)	ConfGen	ConfGen
Ionization state of MaR1 and DHA	Carboxylate anion (−1)	Carboxylate anion (−1)	Carboxylate anion (−1)
Docking protocol			
Stage 1: rapid screening	Glide SP	Glide SP	Glide SP
Stage 2: refined XP docking	Glide XP (top 10% of SP-ranked poses)	Glide XP (top 10% of SP-ranked poses)	Glide XP (top 10% of SP-ranked poses)
VdW scaling (ligand, XP)	0.80 (non-polar)	0.80 (non-polar)	0.80 (non-polar)
Partial charge cutoff	0.15	0.15	0.15
Maximum XP poses requested per ligand	Up to 10, ranked by XP GScore	Up to 10, ranked by XP GScore	Up to 10, ranked by XP GScore
Post-docking minimization	Yes	Yes	Yes
Validation (redocking RMSD)			
Co-crystallized reference	GW590735 (735)	VSP-77 (V77)	Cholesterol (CLR)
Redocking RMSD / Å	0.36	1.06	0.50
Computational setup			
Execution date	2023-08-10	2023-08-10	2023-08-10
Parameter	PPARα (2P54)	PPARγ (6MS7)	RORα (1N83)
XP output entries returned per ligand	MaR1: 4; DHA: 2	MaR1: 4; DHA: 1	MaR1: 10; DHA: 1
Pose-level rescoring	Prime MM-GBSA	Prime MM-GBSA	Prime MM-GBSA

Parameter	PPARα (2P54)	PPARγ (6MS7)	RORα (1N83)
Pose-selection descriptors	XP GScore (primary); Emodel and pose-level Prime MM-GBSA (supporting)	Same	Same
Structural selection criterion	Occupation of the co-crystallized-ligand-defined pocket	Same	Same
Representative pose	Highest-ranked structurally admissible XP pose used as the MD starting structure	Same	Same

Note: *Grid parameters were extracted directly from Glide input files and grid-generation logs, whereas receptor-preparation properties were verified from the minimized Maestro receptor files. All docking-related calculations were performed using Schrödinger Suite 2020-3. We defined grid centers using the corresponding co-crystallized ligand and reported them as Cartesian coordinates in Å. The top 10% criterion refers to the SP-ranked poses advanced to the XP stage. Glide was configured to write up to 10 XP poses per receptor–ligand pair but returned 4 for PPARα/MaR1, 2 for PPARα/DHA, 4 for PPARγ/MaR1, 1 for PPARγ/DHA, 10 for RORα/MaR1, and 1 for RORα/DHA. Thus, 10 represents the maximum requested output, not a fixed number of poses obtained for every complex. Among the returned XP poses, only those occupying the binding pocket defined by the corresponding co-crystallized ligand were considered structurally admissible. We selected the structurally admissible pose ranked highest by XP GScore as representative. Emodel, Glide's composite within-ligand pose-discrimination term, was examined only as a secondary pose-assessment descriptor and was not used to rank MaR1 against DHA or interpreted as a binding-free-energy estimate. Pose-level Prime MM-GBSA was evaluated separately as an additional relative energetic descriptor. When Glide returned only one XP pose, as for RORα/DHA and PPARγ/DHA, we retained the pocket-compatible pose as a structurally admissible starting configuration for MD; in these cases, Emodel could not be used to discriminate among alternative poses. We used each selected pose to initiate four independent molecular dynamics simulations. Abbreviations: SP, Standard Precision; XP, Extra Precision; VdW, van der Waals; RMSD, root-mean-square deviation; MM-GBSA, molecular mechanics/generalized Born surface area.*

Table S4. SiteMap descriptors of the co-crystallized-ligand-centered sites in the prepared PPARα, PPARγ, and RORα structures.

Receptor	SiteScore	Dscore	Site points	Volume (Å³)	Exposure	Enclosure	Contact	Hydrophobic	Hydrophilic	Balance	Donor/acceptor
PPARα	1.043	1.073	167	357.75	0.577	0.735	0.955	0.771	0.945	0.816	1.132

PPARγ	1.079	1.112	137	256.56	0.475	0.774	1.022	1.613	0.896	1.800	0.696
RORα	0.825	0.629	56	126.57	0.533	0.712	1.059	0.125	1.538	0.081	0.580

Note: *SiteMap calculations were performed on the prepared receptor structures and restricted to the site defined by the corresponding co-crystallized ligand: GW590735 for PPARα, (S)-VSP-77 for PPARγ, and cholesterol for RORα. Site points indicate the number of points assigned to the identified site, whereas the remaining columns report the corresponding SiteMap descriptors. The reported volumes describe the co-crystallized-ligand-centered SiteMap sites under this operational definition and should not be interpreted as measurements of the complete anatomical ligand-binding cavities. Values were used descriptively to compare site size and physicochemical character across the three receptor templates.*

Table S5. Binding-pocket residue inventory of the three receptor templates, grouped by structural region.

Receptor	Region	Residue	Physicochemical Class	Minimum distance to the co-crystallized ligand (Å)	Within 5.0 Å	Literature-supported polar anchor
PPARα	Arm I	Phe273	apolar	3.57	yes	no
PPARα	Arm I	Gln277	polar	3.65	yes	no
PPARα	Arm I	Ser280	polar	2.76	yes	yes
PPARα	Arm I	Tyr314	polar	2.72	yes	yes
PPARα	Arm I	Ile317	apolar	4.70	yes	no
PPARα	Arm I	Phe318	apolar	3.98	yes	no
PPARα	Arm I	Ile354	apolar	3.58	yes	no
PPARα	Arm I	His440	polar	2.85	yes	yes
PPARα	Arm I	Val444	apolar	3.84	yes	no
PPARα	Arm I	Leu456	apolar	4.40	yes	no
PPARα	Arm I	Leu460	apolar	3.47	yes	no
PPARα	Arm I	Tyr464	polar	2.68	yes	yes

Receptor	Region	Residue	Physicochemical Class	Minimum distance to the co-crystallized ligand (Å)	Within 5.0 Å	Literature-supported polar anchor
PPARα	Arm II	Glu251	polar	3.56	yes	no
PPARα	Arm II	Leu254	apolar	3.80	yes	no
PPARα	Arm II	Val255	apolar	3.09	yes	no
PPARα	Arm II	Ile272	apolar	4.49	yes	no
PPARα	Arm II	Cys275	polar	3.63	yes	no
PPARα	Arm II	Cys276	polar	3.48	yes	no
PPARα	Arm II	Thr279	polar	3.42	yes	no
PPARα	β-sheet region	Ile241	apolar	3.41	yes	no
PPARα	β-sheet region	Leu247	apolar	4.35	yes	no
PPARα	β-sheet region	Ala250	apolar	3.83	yes	no
PPARα	β-sheet region	Leu321	apolar	3.77	yes	no
PPARα	β-sheet region	Met330	apolar	3.82	yes	no
PPARα	β-sheet region	Val332	apolar	3.45	yes	no
PPARα	β-sheet region	Ala333	apolar	4.31	yes	no
PPARα	β-sheet region	Ile339	apolar	3.94	yes	no
PPARα	β-sheet region	Leu344	apolar	3.99	yes	no
PPARα	β-sheet region	Met355	apolar	3.56	yes	no
PPARγ	Arm I	Ser289	polar	3.90	yes	yes
PPARγ	Arm I	Ala292	apolar	3.54	yes	no

Receptor	Region	Residue	Physicochemical Class	Minimum distance to the co-crystallized ligand (Å)	Within 5.0 Å	Literature-supported polar anchor
PPARγ	Arm I	Ile296	apolar	4.32	yes	no
PPARγ	Arm I	His323	polar	4.60	yes	yes
PPARγ	Arm I	Ile326	apolar	3.79	yes	no
PPARγ	Arm I	Tyr327	polar	3.68	yes	no
PPARγ	Arm I	His449	polar	4.10	yes	yes
PPARγ	Arm I	Tyr473	polar	5.49	no	yes
PPARγ	Arm II	Phe226	apolar	3.68	yes	no
PPARγ	Arm II	Cys285	polar	3.47	yes	no
PPARγ	Arm II	Glu295	polar	3.64	yes	no
PPARγ	Arm II	Met329	apolar	3.68	yes	no
PPARγ	Arm II	Leu330	apolar	4.18	yes	no
PPARγ	Arm II	Met364	apolar	3.86	yes	no
PPARγ	β-sheet region	Arg288	polar	2.85	yes	yes
PPARγ	β-sheet region	Leu333	apolar	3.78	yes	no
PPARγ	β-sheet region	Leu340	apolar	4.62	yes	no
PPARγ	β-sheet region	Ile341	apolar	3.43	yes	no
PPARγ	β-sheet region	Ser342	polar	3.17	yes	no
PPARγ	β-sheet region	Glu343	polar	4.04	yes	yes
RORα	polar entrance	Gln289	polar	5.81	no	yes

Receptor	Region	Residue	Physicochemical Class	Minimum distance to the co-crystallized ligand (Å)	Within 5.0 Å	Literature-supported polar anchor
RORα	polar entrance	Tyr290	polar	6.49	no	yes
RORα	polar entrance	Ala330	apolar	3.64	yes	no
RORα	polar entrance	Arg367	polar	3.75	yes	yes
RORα	polar entrance	Arg370	polar	4.94	yes	yes
RORα	polar entrance	Tyr380	polar	3.31	yes	no
RORα	hydrophobic body	Trp320	apolar	3.45	yes	no
RORα	hydrophobic body	Cys323	polar	3.83	yes	no
RORα	hydrophobic body	Ala324	apolar	4.77	yes	no
RORα	hydrophobic body	Lys326	polar	3.19	yes	no
RORα	hydrophobic body	Ile327	apolar	3.84	yes	no
RORα	hydrophobic body	Val364	apolar	3.34	yes	no
RORα	hydrophobic body	Phe365	apolar	4.13	yes	no
RORα	hydrophobic body	Met368	apolar	3.72	yes	no

Receptor	Region	Residue	Physicochemical Class	Minimum distance to the co-crystallized ligand (Å)	Within 5.0 Å	Literature-supported polar anchor
RORα	hydrophobic body	Ala371	apolar	4.10	yes	no
RORα	hydrophobic body	Val379	apolar	3.87	yes	no
RORα	hydrophobic body	Phe381	apolar	3.83	yes	no
RORα	hydrophobic body	Phe391	apolar	3.70	yes	no
RORα	hydrophobic body	Leu394	apolar	3.53	yes	no
RORα	hydrophobic body	Cys396	polar	4.93	yes	no
RORα	hydrophobic body	Phe399	apolar	3.74	yes	no
RORα	hydrophobic body	Ile400	apolar	3.91	yes	no
RORα	hydrophobic body	Val403	apolar	3.64	yes	no
RORα	hydrophobic body	His484	polar	4.04	yes	no
RORα	hydrophobic body	Tyr507	polar	3.89	yes	no

Note: *Pocket-lining residues were identified in the prepared receptor structures using the corresponding co-crystallized ligand as the spatial reference: GW590735 for PPARα, (S)-VSP-77 for PPARγ, and cholesterol for RORα. Unless otherwise indicated, listed residues contained at least one heavy atom*

within 5.0 Å of the corresponding co-crystallized ligand; reported distances represent the minimum heavy-atom distance between the residue and ligand. Residues were classified as polar or apolar according to their side-chain physicochemical character. For PPARα and PPARγ, the β-sheet region comprised residues assigned to a β-strand by DSSP together with residues containing a heavy atom within 4.0 Å of that strand. Among the remaining residues, Arm I comprised those closer to the AF-2 tyrosine—Tyr464 in PPARα or Tyr473 in PPARγ—than to the β-sheet region, whereas Arm II comprised the remaining pocket residues. Because RORα lacks the branched PPAR architecture, its pocket was divided into a polar entrance and a hydrophobic body. Literature-supported polar anchoring residues were retained even when they fell beyond the 5.0 Å cutoff; these exceptions were Tyr473 in PPARγ and Gln289 and Tyr290 in RORα. Distances in this table characterize the prepared crystallographic receptor templates and should not be interpreted as MaR1- or DHA-contact occupancies.

Table S6. Ligand conformational-sampling census and Glide XP pose-selection funnel.

System	Rotatable bonds	ConfGen conformers retained	XP poses written	Selected-pose XP GScore (kcal·mol^{-1})	Selected-pose Emodel (kcal·mol^{-1})
RORα/MaR1	16	64	10	−10.165	−55.155
RORα/DHA	14	64	1	−9.058	−38.623
PPARα/MaR1	16	64	4	−10.174	−64.406
PPARα/DHA	14	64	2	−5.422	−47.772
PPARγ/MaR1	16	64	4	−10.502	−74.708
PPARγ/DHA	14	64	1	−9.434	−54.033

Note: *Rotatable-bond and retained-conformer counts were obtained from an exhaustive ConfGen search of the LigPrep-prepared ligands and describe the accessible ligand conformational space before docking. Glide generates its own conformers during docking; therefore, these values do not represent the internal conformational sampling performed by Glide. Glide was configured to write up to 10 XP poses per receptor–ligand pair, whereas the XP poses written column reports the number of output entries actually returned for each system. Among the returned poses, only those occupying the binding pocket defined by the corresponding co-crystallized ligand were considered structurally admissible. The structurally admissible pose ranked highest by XP GScore was selected as the representative pose. XP GScore and Emodel values therefore correspond to the selected poses reported in Table 2 of the main manuscript. Emodel was examined only as a secondary within-ligand pose-assessment descriptor and was not used to rank chemically distinct ligands or estimate binding affinity. When only one XP pose was returned, as for RORα/DHA and PPARγ/DHA, Emodel could not discriminate among alternative poses.*

Table S7. Per-replica Cα RMSD and Cα RMSF statistics from the full 250 ns molecular dynamics trajectories of the six receptor–ligand complexes.

Panel A: Protein backbone Cα RMSD per replica.

Complex	Rep-1	Rep-2	Rep-3	Rep-4	Four-replica mean ± SD
RORα/MaR1	1.80 ± 0.28	1.99 ± 0.28	2.34 ± 0.74	1.81 ± 0.26	1.98 ± 0.25
RORα/DHA	2.19 ± 0.44	1.61 ± 0.21	2.04 ± 0.31	1.89 ± 0.25	1.93 ± 0.25
PPARα/MaR1	2.49 ± 0.20	2.47 ± 0.35	2.10 ± 0.16	2.01 ± 0.16	2.27 ± 0.25
PPARα/DHA	2.08 ± 0.15	2.30 ± 0.21	2.08 ± 0.19	2.20 ± 0.21	2.16 ± 0.11
PPARγ/MaR1	2.02 ± 0.30	1.95 ± 0.17	1.98 ± 0.19	1.83 ± 0.16	1.94 ± 0.08
PPARγ/DHA	2.52 ± 0.44	2.29 ± 0.26	2.58 ± 0.48	2.57 ± 0.33	2.49 ± 0.13

Panel B: Per-residue Cα RMSF per replica.

Complex	Rep-1	Rep-2	Rep-3	Rep-4	Four-replica mean ± SD
RORα/MaR1	0.94 ± 0.78	0.96 ± 0.79	1.20 ± 1.39	0.98 ± 0.93	1.02 ± 0.13
RORα/DHA	1.02 ± 1.09	0.97 ± 0.74	1.04 ± 1.03	1.05 ± 0.81	1.02 ± 0.04
PPARα/MaR1	1.12 ± 0.61	1.09 ± 0.58	0.96 ± 0.49	0.93 ± 0.48	1.03 ± 0.09
PPARα/DHA	0.93 ± 0.52	1.11 ± 0.63	0.98 ± 0.46	0.99 ± 0.49	1.00 ± 0.07
PPARγ/MaR1	1.02 ± 0.63	0.99 ± 0.59	1.05 ± 0.68	1.01 ± 0.59	1.02 ± 0.02
PPARγ/DHA	1.32 ± 0.83	1.30 ± 1.04	1.28 ± 0.63	1.16 ± 0.63	1.27 ± 0.07

Note: *For Panel A, values for each replica represent the mean ± SD of protein backbone Cα RMSD values calculated over the 250 ns production trajectory after alignment to the initially minimized structure. For Panel B, values for each replica represent the mean ± SD of per-residue Cα RMSF values calculated*

across the ligand-binding domain. The final column reports the mean of the four replica means ± sample standard deviation. RMSD and RMSF values are reported in Å. Figure S3A and Figure S4 show the corresponding time-series and per-residue profiles, respectively.

Table S8. Replica-level total protein–ligand contact occupancies across four independent 250 ns molecular dynamics replicas of the six receptor–ligand complexes.

Computational details. Per-residue protein–ligand contact occupancies were calculated independently for each of the four 250 ns replicas of every receptor–ligand complex using the corresponding Schrödinger Desmond Simulation Interaction Diagram outputs. The analyzed contact categories included hydrogen bonds, hydrophobic contacts, ionic interactions, and water bridges. For each residue, total occupancy was defined as the percentage of trajectory frames containing at least one classified protein–ligand interaction. We counted multiple contact categories involving the same residue within a single frame once; total occupancy therefore ranged from 0 to 100%. Tables S8a–S8f report the four independent replica occupancies together with their arithmetic mean and sample standard deviation. We excluded concatenated values from these replica-level summaries. Only residues with a mean total occupancy ≥5% across the four replicas are shown. Residue numbering corresponds to the receptor constructs used in the simulations.

Table S8a. Replica-level total protein–ligand contact occupancies for PPARα/DHA.

Residue	Rep-1 (%)	Rep-2 (%)	Rep-3 (%)	Rep-4 (%)	Mean (%)	SD (%)
Cys276	99.8	99.5	98.6	99.7	99.4	0.6
Val332	99.7	99.8	97.4	97.0	98.5	1.5
HIE440	94.8	99.9	95.7	98.8	97.3	2.4
Tyr314	89.4	100.0	99.7	85.6	93.6	7.3
Met330	96.2	89.9	97.3	86.2	92.4	5.3
Ile339	94.9	84.6	94.0	87.0	90.1	5.1
Met355	90.6	88.5	79.4	99.1	89.4	8.1
Ser280	78.2	98.2	96.9	79.9	88.3	10.7
Cys275	82.6	96.4	83.8	83.6	86.6	6.6
Ile354	95.6	56.2	89.8	97.6	84.8	19.4

Residue	Rep-1 (%)	Rep-2 (%)	Rep-3 (%)	Rep-4 (%)	Mean (%)	SD (%)
Ile272	84.4	84.6	76.0	93.9	84.7	7.3
Thr279	89.5	86.8	99.4	57.4	83.3	18.1
Tyr464	79.6	94.7	91.3	36.8	75.6	26.7
Lys358	64.4	84.8	90.4	51.5	72.8	18.1
Gln277	73.3	64.6	64.6	70.2	68.2	4.3
Leu321	95.3	31.6	92.6	46.6	66.5	32.3
Leu247	50.7	86.8	65.2	62.3	66.3	15.0
Phe273	86.6	28.5	51.4	95.3	65.5	31.1
Leu258	76.1	5.8	75.4	64.8	55.5	33.6
Val255	57.4	2.6	72.2	75.4	51.9	33.8
Phe318	30.6	89.6	55.9	24.1	50.0	29.7
Ile241	62.1	57.2	63.9	12.6	49.0	24.4
Leu254	1.4	82.3	3.3	72.9	40.0	43.6
Met325	25.4	34.2	44.8	50.7	38.8	11.2
Leu460	26.8	60.3	56.5	3.2	36.7	26.9
Ile317	73.3	4.4	58.8	0.8	34.3	37.2
Phe359	11.4	40.9	27.2	28.1	26.9	12.1
Ala250	4.3	82.5	10.2	0.3	24.3	39.0
Val444	5.2	13.7	1.0	62.3	20.6	28.3
Phe343	0.8	4.2	11.0	46.5	15.6	21.1
Ala333	1.2	34.0	0.8	23.0	14.7	16.5

Residue	Rep-1 (%)	Rep-2 (%)	Rep-3 (%)	Rep-4 (%)	Mean (%)	SD (%)
Glu251	2.4	55.9	0.1	0.0	14.6	27.5
Met220	48.1	0.0	0.0	1.3	12.3	23.8
Leu344	17.2	16.6	7.0	6.3	11.8	5.9
Ile447	0.7	0.1	0.0	27.9	7.2	13.8
Leu347	0.0	0.0	0.0	24.9	6.2	12.4
Phe351	0.9	0.0	0.0	23.5	6.1	11.6

Table S8b. Replica-level total protein–ligand contact occupancies for PPARα/MaR1.

Residue	Rep-1 (%)	Rep-2 (%)	Rep-3 (%)	Rep-4 (%)	Mean (%)	SD (%)
Cys276	99.8	99.9	100.0	99.9	99.9	0.1
Val332	98.4	99.2	99.8	98.5	99.0	0.6
Ile354	99.6	99.1	95.4	93.6	96.9	2.9
HIE440	94.1	98.3	96.1	97.6	96.5	1.9
Tyr314	83.8	99.8	99.5	99.8	95.8	8.0
Ser280	87.5	92.6	96.3	97.9	93.6	4.6
Gln277	98.8	95.1	90.6	88.8	93.3	4.5
Lys358	99.4	99.1	72.7	98.0	92.3	13.1
Ile339	87.4	96.0	97.0	88.7	92.3	4.9
Phe273	93.8	98.6	98.4	78.2	92.3	9.6
Met355	97.1	90.6	86.2	89.2	90.8	4.6
Cys275	74.5	97.4	91.2	95.8	89.7	10.5

Residue	Rep-1 (%)	Rep-2 (%)	Rep-3 (%)	Rep-4 (%)	Mean (%)	SD (%)
Met330	55.9	92.5	97.6	97.7	85.9	20.2
Thr279	41.5	75.2	99.6	97.3	78.4	26.9
Ile272	93.7	55.3	89.3	73.5	77.9	17.4
Leu247	71.9	91.4	64.5	54.7	70.6	15.5
Ile241	63.5	73.7	87.5	27.6	63.1	25.6
Leu460	60.1	57.7	63.9	65.7	61.8	3.6
Val255	5.3	88.9	51.6	74.3	55.0	36.5
Leu321	6.9	5.2	98.0	95.6	51.4	52.4
Tyr464	16.0	13.1	97.0	65.4	47.9	40.6
Val444	62.1	63.3	2.9	41.9	42.5	28.2
Ala250	61.2	82.6	11.5	9.4	41.2	36.5
Leu331	0.0	0.0	78.4	59.5	34.5	40.5
Phe359	68.6	59.3	0.0	0.0	32.0	37.1
Leu258	1.9	23.9	82.9	16.3	31.3	35.6
Met325	13.8	34.8	62.5	8.4	29.8	24.6
Leu254	75.2	38.5	0.2	0.5	28.6	35.9
Glu251	50.5	26.5	1.6	5.2	21.0	22.5
Leu344	11.5	61.3	1.0	8.1	20.5	27.6
Ile317	0.0	0.1	0.0	49.8	12.5	24.9
Val324	0.0	0.0	39.5	9.1	12.2	18.8
Ala256	38.9	0.0	0.0	0.0	9.7	19.5
Ala333	28.8	3.0	0.3	1.1	8.3	13.7

Residue	Rep-1 (%)	Rep-2 (%)	Rep-3 (%)	Rep-4 (%)	Mean (%)	SD (%)
Thr283	0.0	0.0	0.0	28.6	7.1	14.3

Table S8c. Replica-level total protein–ligand contact occupancies for PPARγ/DHA.

Residue	Rep-1 (%)	Rep-2 (%)	Rep-3 (%)	Rep-4 (%)	Mean (%)	SD (%)
Leu330	99.4	98.6	99.0	99.7	99.2	0.5
Cys285	95.2	99.8	99.4	99.4	98.4	2.2
Arg288	98.7	96.4	96.6	99.9	97.9	1.7
Ile326	88.3	98.3	97.3	99.2	95.8	5.1
Phe363	89.1	96.8	55.0	96.6	84.4	19.9
HIE449	80.8	84.8	84.6	85.8	84.0	2.2
Met364	68.9	89.7	86.4	88.0	83.2	9.7
Phe282	33.0	95.8	97.0	83.8	77.4	30.2
Leu333	79.1	60.6	66.3	92.4	74.6	14.2
Tyr327	84.9	57.4	68.1	58.1	67.1	12.8
Ile341	87.5	49.5	82.7	31.1	62.7	27.0
Met329	60.0	94.5	26.1	68.7	62.3	28.2
Ser342	86.6	41.2	91.8	22.4	60.5	34.1
Gln286	52.6	37.1	92.2	58.7	60.2	23.2
Ser289	61.9	31.5	53.6	79.2	56.5	19.8
Ile281	15.8	77.5	50.3	79.0	55.7	29.7
Phe360	0.0	68.6	36.9	68.5	43.5	32.6
Ala292	55.7	74.0	3.5	33.5	41.7	30.4
Leu356	0.0	68.3	38.5	59.7	41.6	30.4
Leu453	26.3	27.7	56.9	30.6	35.4	14.4
Leu353	24.2	44.7	22.6	46.6	34.5	12.9
Val339	71.1	7.1	32.7	17.5	32.1	28.1
Leu469	32.0	0.6	70.7	24.7	32.0	29.1
Tyr473	30.1	0.2	66.5	30.6	31.9	27.1

Residue	Rep-1 (%)	Rep-2 (%)	Rep-3 (%)	Rep-4 (%)	Mean (%)	SD (%)
Lys367	70.0	3.8	23.5	24.3	30.4	28.0
Met348	48.3	9.3	21.7	18.0	24.3	16.8
Glu343	31.3	31.7	8.6	17.8	22.3	11.2
Leu465	21.6	0.1	52.3	14.7	22.2	22.0
Phe368	47.2	0.7	28.9	7.0	20.9	21.3
Phe226	0.0	56.7	1.1	0.6	14.6	28.1
Met334	28.4	2.2	2.0	16.8	12.4	12.8
Leu452	0.3	0.4	14.0	29.4	11.0	13.8
Leu228	11.4	5.5	9.2	16.4	10.6	4.6
Glu295	0.1	37.1	0.0	0.6	9.5	18.4
Ile456	0.5	8.1	13.5	10.6	8.2	5.6
Ala278	0.0	8.4	8.0	7.2	5.9	4.0
Ile296	0.0	21.6	0.0	0.0	5.4	10.8

Table S8d. Replica-level total protein–ligand contact occupancies for PPARγ/MaR1.

Residue	Rep-1 (%)	Rep-2 (%)	Rep-3 (%)	Rep-4 (%)	Mean (%)	SD (%)
Leu330	100.0	99.5	99.4	99.6	99.6	0.2
Ile326	99.1	98.8	98.2	97.4	98.4	0.8
Leu333	97.8	92.9	98.7	98.0	96.9	2.6
Cys285	99.3	99.4	85.1	96.8	95.2	6.8
Gln286	93.6	96.6	90.2	92.7	93.3	2.7
Arg288	97.7	86.0	76.2	96.6	89.1	10.1
Met329	89.0	85.0	88.4	90.4	88.2	2.3
Ala292	74.6	70.0	91.3	92.0	82.0	11.3
HIE449	98.8	36.1	89.9	99.1	81.0	30.2

Residue	Rep-1 (%)	Rep-2 (%)	Rep-3 (%)	Rep-4 (%)	Mean (%)	SD (%)
Ser289	84.9	76.8	81.1	72.8	78.9	5.2
Tyr473	36.9	85.1	88.2	100.0	77.5	27.9
Phe363	98.7	42.9	97.5	70.5	77.4	26.4
HIE323	83.4	38.2	70.6	95.0	71.8	24.5
Phe282	73.7	56.7	56.3	97.6	71.1	19.5
Met364	43.3	56.9	50.7	76.5	56.8	14.2
Ile341	40.4	45.1	45.9	80.3	52.9	18.4
Lys367	69.0	18.8	67.8	52.3	51.9	23.4
Tyr327	87.8	9.1	91.9	11.6	50.1	45.9
Leu469	51.4	78.8	4.9	63.5	49.7	31.9
Leu228	67.9	2.9	79.8	38.2	47.2	34.3
Leu453	17.2	96.0	21.9	43.0	44.5	36.1
Phe226	11.6	0.8	72.0	81.6	41.5	41.2
Val339	9.8	93.1	2.4	54.7	40.0	42.2
Ser342	59.5	31.1	29.9	30.1	37.6	14.6
Leu340	7.7	87.8	0.4	42.5	34.6	40.0
Glu343	60.0	0.0	37.5	17.0	28.6	25.9
Met348	1.7	62.4	0.4	34.5	24.8	29.6
Lys457	0.0	91.6	0.0	0.0	22.9	45.8
Met463	0.0	56.8	0.0	23.3	20.0	26.9
Pro227	0.8	0.0	42.7	20.6	16.0	20.2
Leu465	51.4	2.7	8.4	0.0	15.6	24.1

Residue	Rep-1 (%)	Rep-2 (%)	Rep-3 (%)	Rep-4 (%)	Mean (%)	SD (%)
Glu295	2.4	0.0	37.9	2.6	10.7	18.1
Phe368	0.0	0.2	0.0	33.6	8.5	16.8
Glu291	0.9	0.0	27.9	4.2	8.2	13.3

Table S8e. Replica-level total protein–ligand contact occupancies for RORα/DHA.

Residue	Rep-1 (%)	Rep-2 (%)	Rep-3 (%)	Rep-4 (%)	Mean (%)	SD (%)
Ile327	97.3	98.0	98.0	97.6	97.7	0.4
Phe399	97.0	95.0	95.6	94.8	95.6	1.0
Met368	95.0	95.0	91.3	97.0	94.6	2.4
Ile400	93.2	91.2	92.6	93.7	92.7	1.1
Phe391	88.8	86.6	89.7	91.0	89.0	1.9
Cys323	87.2	86.1	94.8	87.8	89.0	4.0
Leu394	87.1	85.7	95.3	82.2	87.6	5.6
Val379	91.3	84.4	81.0	86.1	85.7	4.3
His484	84.9	81.7	89.6	83.9	85.0	3.3
Trp320	82.6	82.1	96.2	73.1	83.5	9.5
Gln289	92.3	100.0	98.9	36.8	82.0	30.3
Tyr290	86.7	98.6	96.6	40.5	80.6	27.2
Val364	87.2	82.6	65.7	77.0	78.1	9.3

Residue	Rep-1 (%)	Rep-2 (%)	Rep-3 (%)	Rep-4 (%)	Mean (%)	SD (%)
Ala330	95.0	47.8	77.5	78.2	74.6	19.6
Phe381	85.2	71.3	72.1	68.9	74.4	7.3
Ala371	35.3	94.8	90.8	74.0	73.7	27.1
Arg367	89.2	22.7	98.0	80.8	72.7	34.1
Val403	72.2	55.5	66.4	63.9	64.5	6.9
Arg370	8.8	100.0	100.0	27.5	59.1	47.9
Lys326	71.5	23.5	62.4	76.4	58.4	24.0
Phe365	44.3	49.2	54.5	58.7	51.7	6.2
Cys396	34.9	39.3	35.5	30.4	35.0	3.7
Phe404	42.0	21.8	32.5	38.2	33.6	8.8
Leu295	6.7	84.9	11.0	22.8	31.4	36.4
Tyr380	6.7	67.9	2.2	48.0	31.2	32.0
Cys288	3.0	84.1	21.4	1.8	27.6	38.7
Lys487	18.4	24.2	14.7	10.6	17.0	5.8
Tyr333	8.7	0.0	0.0	55.3	16.0	26.5
Tyr507	11.9	8.8	17.7	3.3	10.4	6.0
Ala324	6.2	5.2	8.4	3.7	5.9	2.0

Table S8f. Replica-level total protein–ligand contact occupancies for RORα/MaR1.

Residue	Rep-1 (%)	Rep-2 (%)	Rep-3 (%)	Rep-4 (%)	Mean (%)	SD (%)
Ile327	97.9	95.3	97.8	97.1	97.0	1.2
Ala371	91.3	96.0	88.8	98.3	93.6	4.3
Phe391	98.6	92.0	82.0	94.6	91.8	7.1
Tyr290	68.7	98.4	95.6	94.9	89.4	13.9
Phe399	73.1	93.1	95.3	90.0	87.9	10.1
Met368	90.1	83.0	94.0	83.3	87.6	5.4
Ile400	80.7	87.7	89.3	87.9	86.4	3.9
Val379	83.9	92.2	93.2	72.5	85.5	9.6
Arg370	39.7	100.0	100.0	100.0	84.9	30.2
Cys323	75.7	88.7	90.6	79.7	83.7	7.1
Gln289	34.5	99.8	100.0	99.9	83.5	32.7
Leu295	58.1	91.5	81.9	94.8	81.6	16.6
Leu394	48.3	83.6	91.3	69.9	73.3	18.9
Tyr380	79.6	88.8	30.7	89.2	72.1	27.9
His484	36.3	81.6	88.6	68.0	68.7	23.2
Phe381	73.2	71.2	60.7	53.0	64.5	9.5
Trp320	9.7	84.6	95.0	64.1	63.3	38.0
Val364	91.4	15.7	73.3	51.6	58.0	32.6
Phe365	94.9	40.6	42.8	47.9	56.6	25.8
Ala330	74.4	8.7	94.1	40.0	54.3	37.7
Val403	74.1	47.5	44.0	46.3	52.9	14.1
Cys288	12.5	76.6	38.8	63.7	47.9	28.3

Residue	Rep-1 (%)	Rep-2 (%)	Rep-3 (%)	Rep-4 (%)	Mean (%)	SD (%)
Lys326	75.8	34.1	16.3	56.9	45.8	26.0
Arg367	92.8	12.1	35.5	32.1	43.1	34.7
Tyr333	79.5	0.7	60.1	0.5	35.2	40.7
Cys396	3.2	41.5	31.9	28.2	26.2	16.3
Lys487	2.6	38.6	13.3	23.0	19.4	15.3
Phe404	12.6	20.2	4.2	20.6	14.4	7.7
Tyr507	2.6	24.4	22.6	6.0	13.9	11.2
Ala324	2.0	17.1	10.8	0.8	7.7	7.7

Note: *Values represent the percentage of trajectory frames containing at least one classified protein–ligand contact involving the indicated residue. We did not sum multiple contact types occurring within the same frame. Mean and sample standard deviation were calculated across four independent 250 ns replicas (n = 4). Contact occupancies describe interaction persistence and should not be interpreted as direct evidence of receptor activation, transcriptional efficacy, or coactivator recruitment.*

Table S9. Ligand oxygen-atom assignments used for the residue–ligand distance analyses.

Ligand	Topology atom(s)	Chemical assignment	Treatment in distance analysis
MaR1	O1	C7-OH	Analyzed individually
MaR1	O2	C14-OH	Analyzed individually
MaR1	O3/O4	Carboxylate group	Minimum distance to either oxygen calculated per frame
DHA	O1/O2	Carboxylate group	Minimum distance to either oxygen calculated per frame

Note: *Atom assignments refer to the ligand atom names in the molecular dynamics topologies analyzed in this study and were verified against chemical connectivity. For carboxylate groups containing two oxygen atoms, the minimum residue–oxygen distance was selected in each frame before replica-level averaging. These distances describe geometric proximity and are not equivalent to hydrogen-bond occupancy.*

Table S10. Replica-level mean residue–ligand oxygen distances used to generate Figure 3.

Complex	Residue–ligand group	Oxygen assignment	R1	R2	R3	R4
PPARα/MaR1	Lys358–C7-OH	O1	3.33	2.82	3.44	2.87
PPARα/MaR1	Tyr314–carboxylate	O3/O4	2.90	2.62	2.72	2.64
PPARα/MaR1	Ser280–carboxylate	O3/O4	3.01	2.88	2.83	2.76
PPARα/MaR1	Tyr464–carboxylate	O3/O4	4.21	4.10	2.70	3.30
PPARα/DHA	Tyr314–carboxylate	O1/O2	2.95	2.70	2.70	3.09
PPARα/DHA	Tyr464–carboxylate	O1/O2	3.05	2.79	2.83	3.71
PPARα/DHA	Ser280–carboxylate	O1/O2	3.49	2.76	3.37	3.17
PPARγ/MaR1	Tyr473–carboxylate	O3/O4	4.87	3.13	4.73	2.66
PPARγ/MaR1	HIE323–carboxylate	O3/O4	3.13	6.03	3.33	2.89
PPARγ/DHA	Arg288–carboxylate	O1/O2	2.99	2.78	2.79	2.70
RORα/MaR1	Gln289–carboxylate	O3/O4	6.93	4.87	4.60	4.89
RORα/MaR1	Arg370–carboxylate	O3/O4	3.82	2.74	2.77	2.75
RORα/MaR1	Arg367–carboxylate	O3/O4	2.82	4.59	4.58	4.48
RORα/MaR1	Lys326–carboxylate	O3/O4	10.78	11.31	12.12	11.01
RORα/DHA	Arg367–carboxylate	O1/O2	3.04	5.21	2.77	3.12
RORα/DHA	Gln289–carboxylate	O1/O2	3.40	4.84	4.62	6.54
RORα/DHA	Arg370–carboxylate	O1/O2	4.89	2.73	2.65	4.21
PPARγ/DHA	Tyr473–carboxylate	O1/O2	16.25	15.07	14.13	13.47

Complex	Residue–ligand group	Oxygen assignment	R1	R2	R3	R4
PPARγ/DHA	HIE323–carboxylate	O1/O2	16.83	15.88	18.50	16.36

Table S11. Numerical parameters and representative-frame identifiers for the global minima of the two-dimensional free-energy landscapes obtained from the replica-balanced 10,000-frame ensembles.

Complex	Frames	RMSD, mean ± SD (nm)	Rg, mean ± SD (nm)	Sampled RMSD range (nm)	Sampled Rg range (nm)	Global minimum RMSD (nm)	Global minimum Rg (nm)	Representative replica	Local frame	Time (ns)
PPARα/MaR1	10000	0.227 ± 0.025	1.887 ± 0.008	0.099–0.330	1.841–1.937	0.203	1.886	R4	2303	230.3
PPARα/DHA	10000	0.216 ± 0.011	1.887 ± 0.004	0.110–0.306	1.858–1.926	0.213	1.884	R4	1355	135.5
PPARγ/MaR1	10000	0.194 ± 0.008	1.905 ± 0.007	0.089–0.265	1.868–1.947	0.193	1.899	R3	174	17.4
PPARγ/DHA	10000	0.249 ± 0.013	1.918 ± 0.005	0.096–0.356	1.873–1.977	0.258	1.916	R3	753	75.3
RORα/MaR1	10000	0.198 ± 0.025	1.911 ± 0.008	0.073–0.396	1.857–1.955	0.168	1.919	R4	145	14.5
RORα/DHA	10000	0.194 ± 0.025	1.920 ± 0.005	0.099–0.311	1.865–1.963	0.168	1.921	R4	1693	169.3

Note: *Values represent the mean ± sample standard deviation of the four independent replica means. We excluded the exact reference frame (frame 0) from each trajectory, yielding 2500 frames per replica and 10,000 equally weighted frames per complex. FELs were generated using RMSD and Rg bin widths of 0.005 and 0.0025 nm, respectively, followed by Gaussian smoothing with σ = 1.5 bins. Representative frames were selected as the observed trajectory frames located closest to the center of the global-minimum FEL bin. Frame numbers and simulation times refer to the indicated individual replica.*

Table S12A. System-level principal component analysis eigenvalues and cumulative explained variance for the six receptor–ligand complexes from the replica-balanced ensemble analyses.

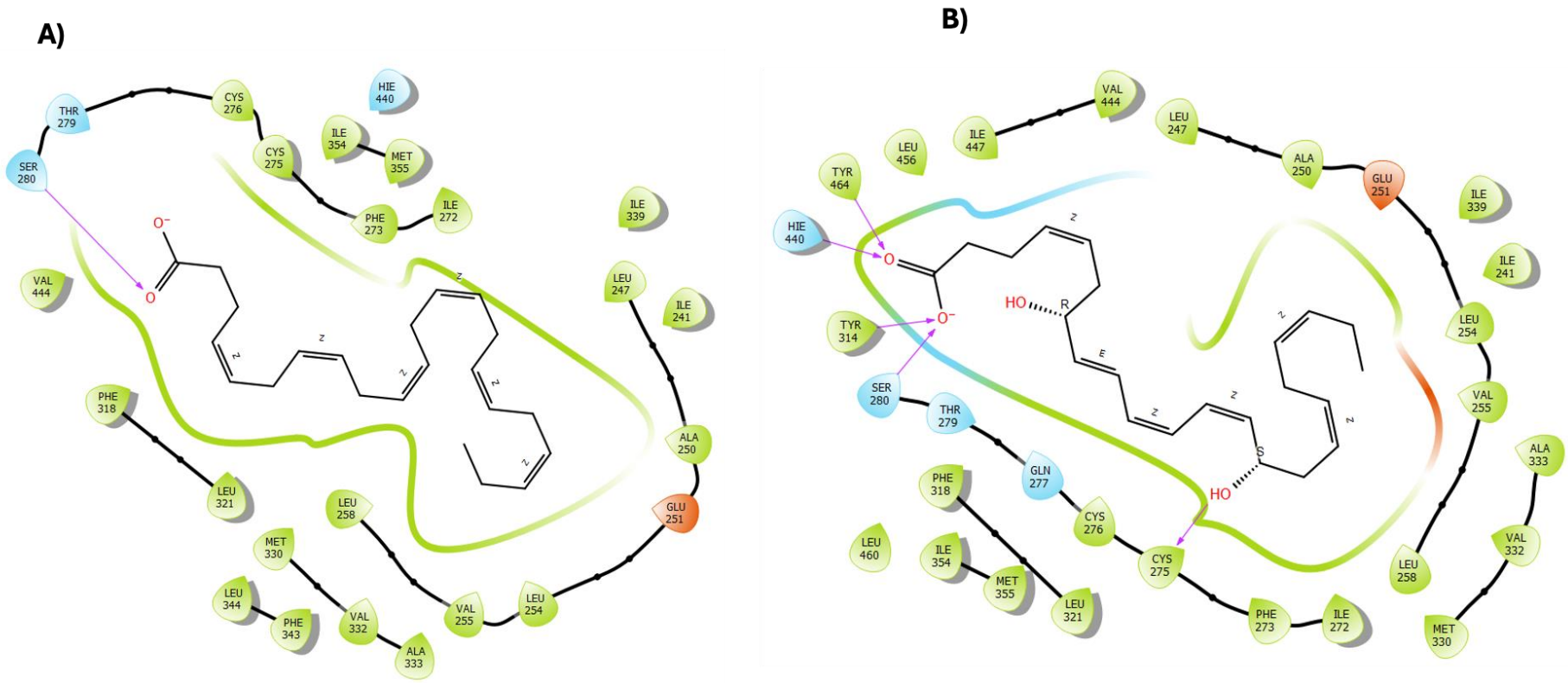
PC	PPARα/MaR1	PPARα/DHA	PPARγ/MaR1	PPARγ/DHA	RORα/MaR1	RORα/DHA
PC1	0.851 / 16.42	1.009 / 19.88	1.145 / 20.63	2.782 / 29.74	2.841 / 41.05	1.734 / 29.50
PC2	0.790 / 31.66	0.693 / 33.53	0.730 / 33.77	1.410 / 44.81	0.969 / 55.05	1.164 / 49.31
PC3	0.396 / 39.29	0.355 / 40.52	0.435 / 41.60	0.705 / 52.35	0.464 / 61.76	0.619 / 59.83
PC4	0.359 / 46.21	0.287 / 46.18	0.303 / 47.06	0.516 / 57.86	0.347 / 66.77	0.288 / 64.72
PC5	0.283 / 51.66	0.278 / 51.66	0.251 / 51.59	0.364 / 61.75	0.257 / 70.48	0.221 / 68.49
PC6	0.192 / 55.37	0.173 / 55.07	0.221 / 55.57	0.325 / 65.22	0.159 / 72.77	0.146 / 70.98
PC7	0.144 / 58.14	0.154 / 58.10	0.205 / 59.26	0.247 / 67.87	0.133 / 74.70	0.118 / 72.98
PC8	0.132 / 60.69	0.137 / 60.79	0.158 / 62.11	0.216 / 70.17	0.109 / 76.27	0.103 / 74.73
PC9	0.114 / 62.90	0.097 / 62.70	0.124 / 64.34	0.184 / 72.14	0.106 / 77.79	0.082 / 76.13
PC10	0.098 / 64.79	0.095 / 64.57	0.110 / 66.31	0.153 / 73.77	0.093 / 79.13	0.075 / 77.40

Note: *Each cell reports the eigenvalue (nm^2) followed by the cumulative percentage of total Cα positional variance explained. Cumulative percentages were calculated using the complete eigenvalue spectrum as the denominator. Eigenvalues and cumulative percentages are reported to three and two decimal places, respectively.*

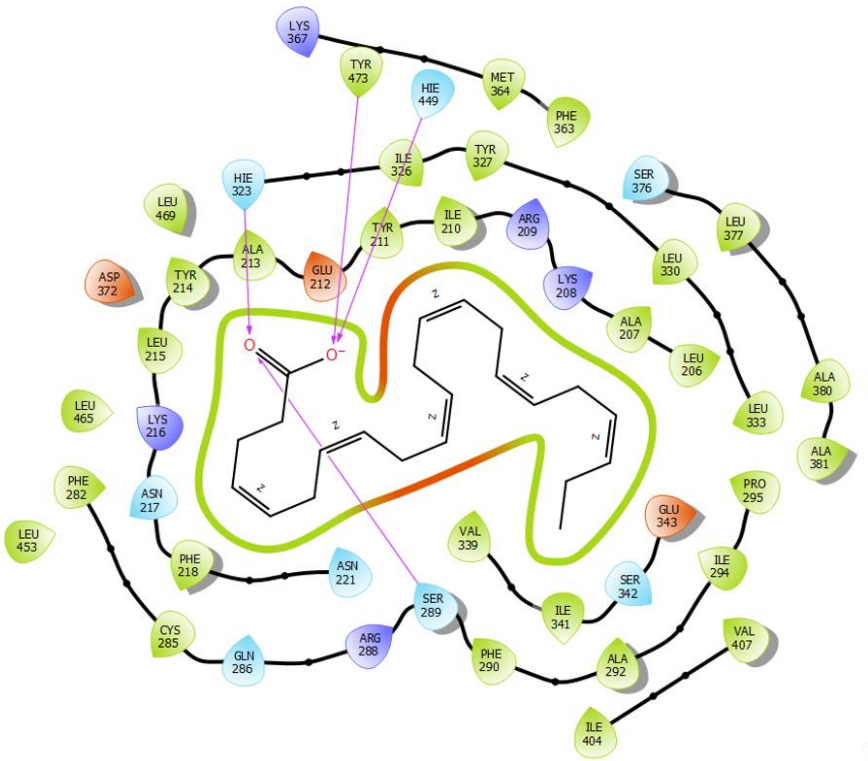
Table S12B. Replica-level PCA cumulative variance and cosine-content metrics across four independent 250 ns trajectories of the six receptor–ligand complexes.

Complex	Replica	PC1 variance (%)	PC2 variance (%)	PC1+PC2 (%)	PC1 cosine content	PC2 cosine content
PPARα/MaR1	R1	23.56	11.97	35.53	0.6957	0.1641
PPARα/MaR1	R2	25.27	12.94	38.21	0.4295	0.3124
PPARα/MaR1	R3	19.93	13.88	33.81	0.6774	0.2707
PPARα/MaR1	R4	18.70	12.84	31.55	0.7557	0.2833
PPARα/MaR1	**Mean ± SD**	**21.87 ± 3.07**	**12.91 ± 0.78**	**34.77 ± 2.81**	**0.6396 ± 0.1440**	**0.2576 ± 0.0647**
PPARα/DHA	R1	17.48	9.34	26.82	0.0266	0.0801
PPARα/DHA	R2	26.58	12.20	38.79	0.7943	0.4224
PPARα/DHA	R3	20.14	9.12	29.26	0.8662	0.0518
PPARα/DHA	R4	18.81	10.15	28.96	0.8708	0.2302
PPARα/DHA	**Mean ± SD**	20.75 ± 4.04	10.20 ± 1.41	30.96 ± 5.33	0.6395 ± 0.4101	0.1961 ± 0.1700
PPARγ/MaR1	R1	31.77	9.46	41.23	0.8274	0.4190
PPARγ/MaR1	R2	21.25	11.40	32.65	0.3847	0.4329
PPARγ/MaR1	R3	16.88	13.60	30.48	0.7950	0.2905
PPARγ/MaR1	R4	21.99	14.27	36.26	0.8968	0.0434
PPARγ/MaR1	**Mean ± SD**	**22.97 ± 6.29**	**12.18 ± 2.19**	**35.16 ± 4.70**	**0.7260 ± 0.2314**	**0.2964 ± 0.1805**
PPARγ/DHA	R1	32.41	17.33	49.74	0.8572	0.7679
PPARγ/DHA	R2	32.22	16.56	48.78	0.6433	0.5012
PPARγ/DHA	R3	45.88	10.82	56.70	0.8852	0.4849
PPARγ/DHA	R4	25.71	10.40	36.11	0.7336	0.4039
PPARγ/DHA	**Mean ± SD**	34.05 ± 8.47	13.78 ± 3.67	47.83 ± 8.57	0.7799 ± 0.1123	0.5395 ± 0.1581
RORα/MaR1	R1	34.06	9.67	43.73	0.0118	0.0060
RORα/MaR1	R2	25.43	15.41	40.84	0.0255	0.0092
RORα/MaR1	R3	55.67	16.14	71.81	0.7762	0.3807
RORα/MaR1	R4	32.56	20.02	52.58	0.0343	0.0001
RORα/MaR1	**Mean ± SD**	**36.93 ± 13.05**	**15.31 ± 4.27**	**52.24 ± 13.97**	**0.2119 ± 0.3763**	**0.0990 ± 0.1878**
RORα/DHA	R1	45.53	14.31	59.85	0.0108	0.1005
RORα/DHA	R2	34.50	13.51	48.01	0.4178	0.0285
RORα/DHA	R3	40.62	18.03	58.65	0.5428	0.0475
RORα/DHA	R4	38.07	13.45	51.51	0.0384	0.0146
RORα/DHA	**Mean ± SD**	39.68 ± 4.64	14.82 ± 2.17	54.50 ± 5.68	0.2524 ± 0.2682	0.0478 ± 0.0377

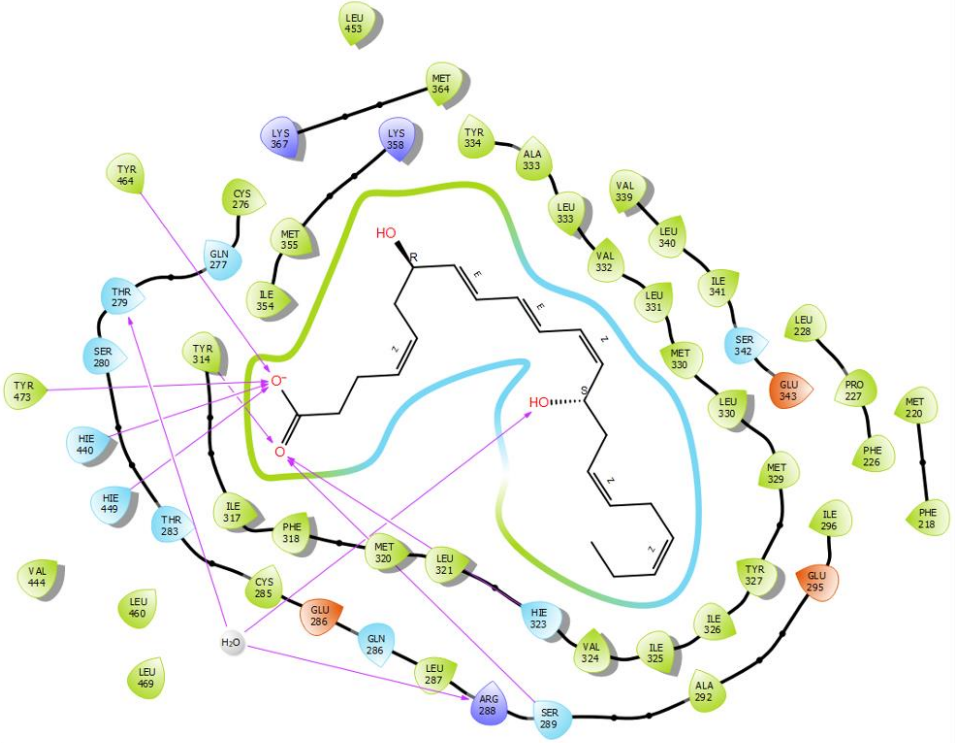
2. Supplementary Figures



C)


LYS 367
TYR 473
HIE 449
MET 364
PHE 363
ILE 326
TYR 327
SER 376
LEU 377
HIE 323
LEU 469
ALA 213
GLU 212
TYR 211
ILE 210
ARG 209
LEU 330
ASP 372
TYR 214
LYS 208
ALA 207
LEU 215
LEU 206
ALA 380
LEU 333
LEU 465
LYS 216
ALA 381
PHE 282
ASN 217
PRO 295
GLU 343
LEU 453
PHE 218
ASN 221
VAL 339
ILE 294
SER 342
SER 289
ILE 341
CYS 285
GLN 286
ARG 288
PHE 290
ALA 292
VAL 407
ILE 404

D)


LEU 453
MET 364
LYS 367
LYS 358
TYR 334
ALA 333
VAL 339
TYR 464
CYS 276
LEU 333
LEU 340
MET 355
GLN 277
VAL 332
ILE 341
THR 279
ILE 354
LEU 331
LEU 228
SER 342
SER 280
TYR 314
MET 330
PRO 227
GLU 343
TYR 473
LEU 330
MET 220
HIE 440
PHE 226
MET 329
HIE 449
ILE 296
ILE 317
THR 283
PHE 318
MET 320
LEU 321
PHE 218
TYR 327
VAL 444
CYS 285
HIE 323
GLU 295
LEU 460
GLU 286
ILE 326
VAL 324
ILE 325
GLN 286
LEU 469
LEU 287
ALA 292
ARG 288
SER 289

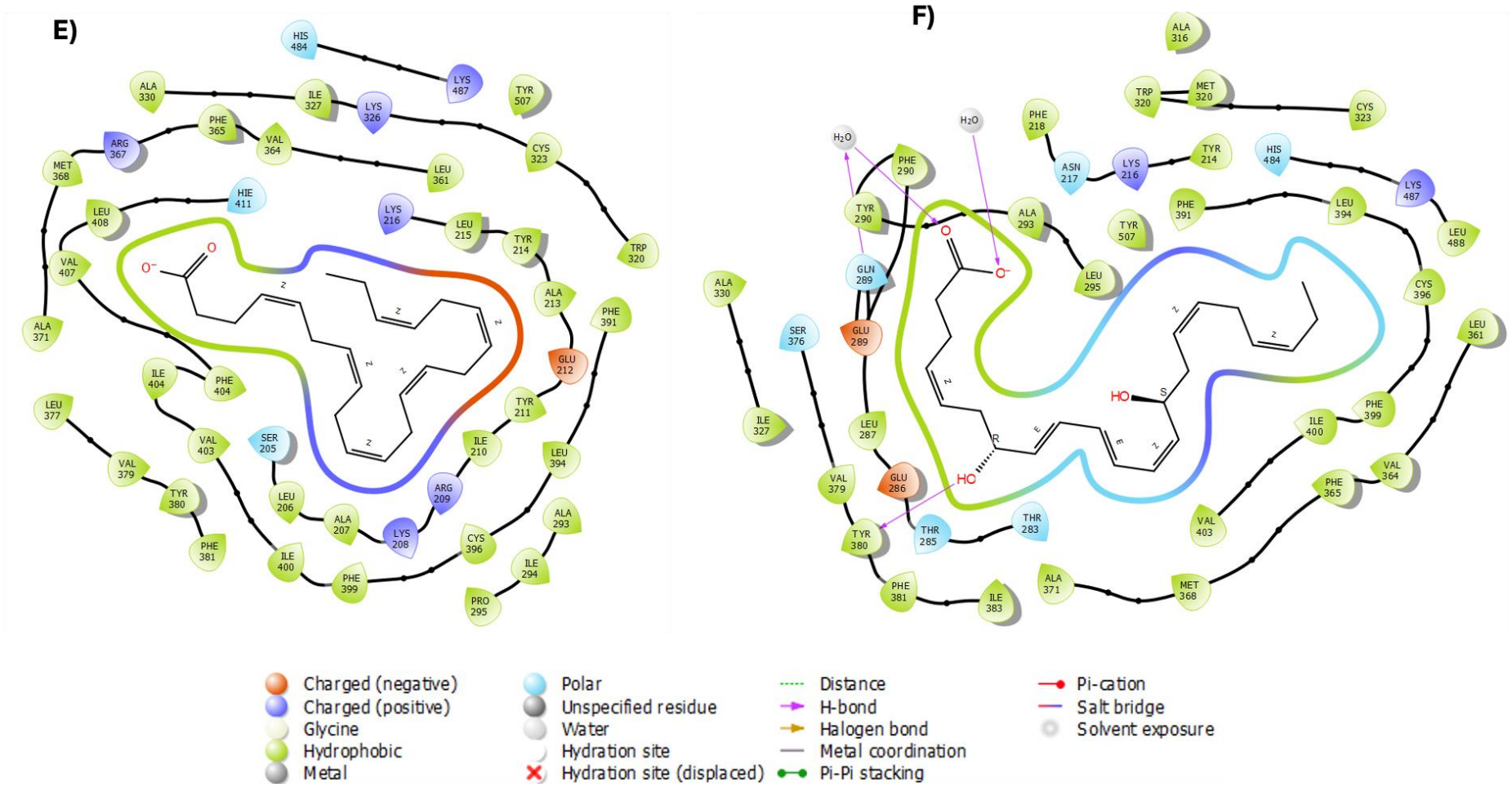


Figure S1. Two-dimensional Glide XP ligand–receptor interaction diagrams of MaR1 and DHA with PPARα, PPARγ, and RORα. The highest-ranked structurally admissible Glide XP poses used as starting structures for the molecular dynamics simulations are shown for each receptor–ligand complex: (A) PPARα/DHA, (B) PPARα/MaR1, (C) PPARγ/DHA, (D) PPARγ/MaR1, (E) RORα/DHA, and (F) RORα/MaR1. Residues within 4 Å of the ligand are displayed. Interaction types and residue properties are color-coded according to Schrödinger conventions, as indicated in the accompanying legend. Residue numbers follow the corresponding PDB structures: PPARα, PDB ID 2P54; PPARγ, PDB ID 6MS7; and RORα, PDB ID 1N83. Diagrams were generated using Maestro v12.5 and Schrödinger Suite 2020-3.

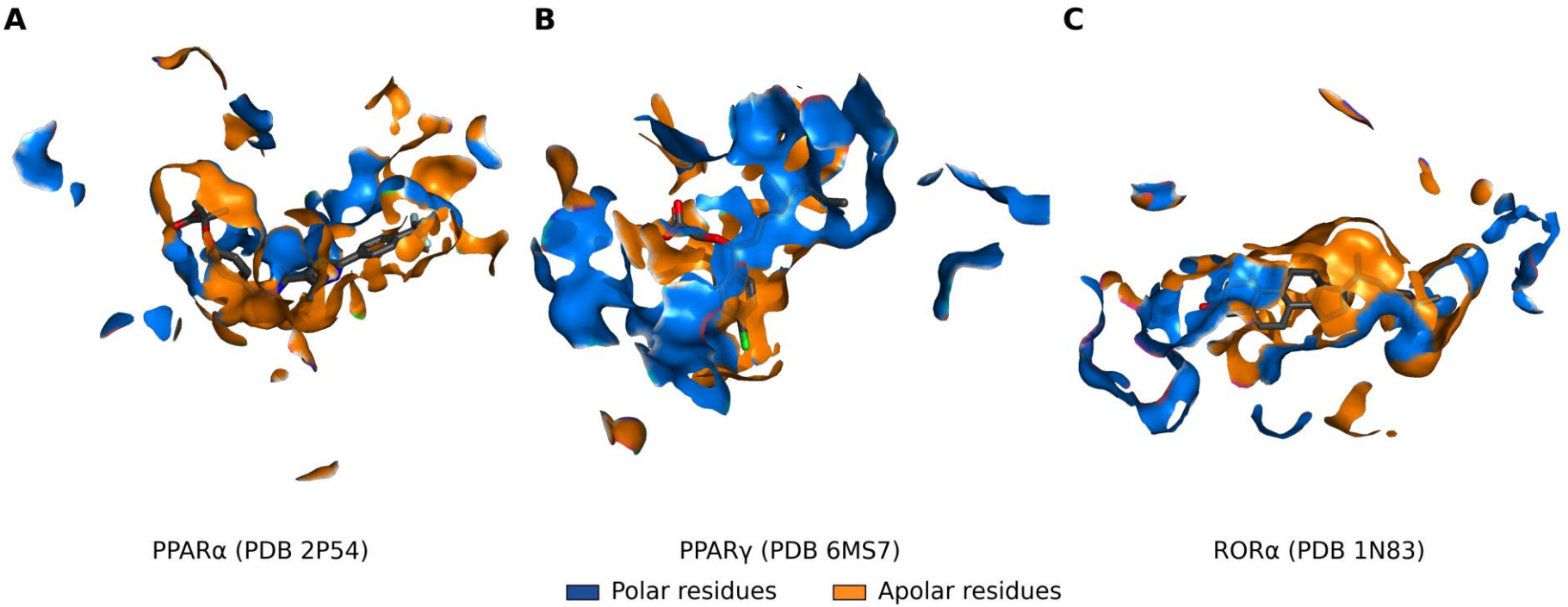


Figure S2. ***Architecture and polarity of the three ligand-binding pockets.*** *Solvent-accessible surfaces were generated from residues lining each pocket, defined as residues containing at least one heavy atom within 6.0 Å of the corresponding co-crystallized ligand. Because Table S5 uses a 5.0 Å cutoff to define the tabulated pocket-residue inventory, it contains a slightly narrower set of residues than the surfaces shown here. Polar residues (Arg, Lys, His, Asp, Glu, Ser, Thr, Asn, Gln, Tyr, and Cys) are shown in blue, whereas apolar residues (Ala, Val, Leu, Ile, Met, Phe, Trp, Pro, and Gly) are shown in orange. Surfaces are displayed at 25% transparency to maintain ligand visibility. The corresponding co-crystallized ligands are shown as gray sticks with oxygen atoms in red: cholesterol in RORα, GW590735 in PPARα, and (S)-VSP-77 in PPARγ. For PPARγ, the (S)-VSP-77 copy assigned as residue 600 in chain A was used, matching the ligand copy analyzed by SiteMap in Table S4. The residue composition of each pocket is reported in Table S5. Images were rendered using PyMOL 3.1.8 at 600 dpi.*

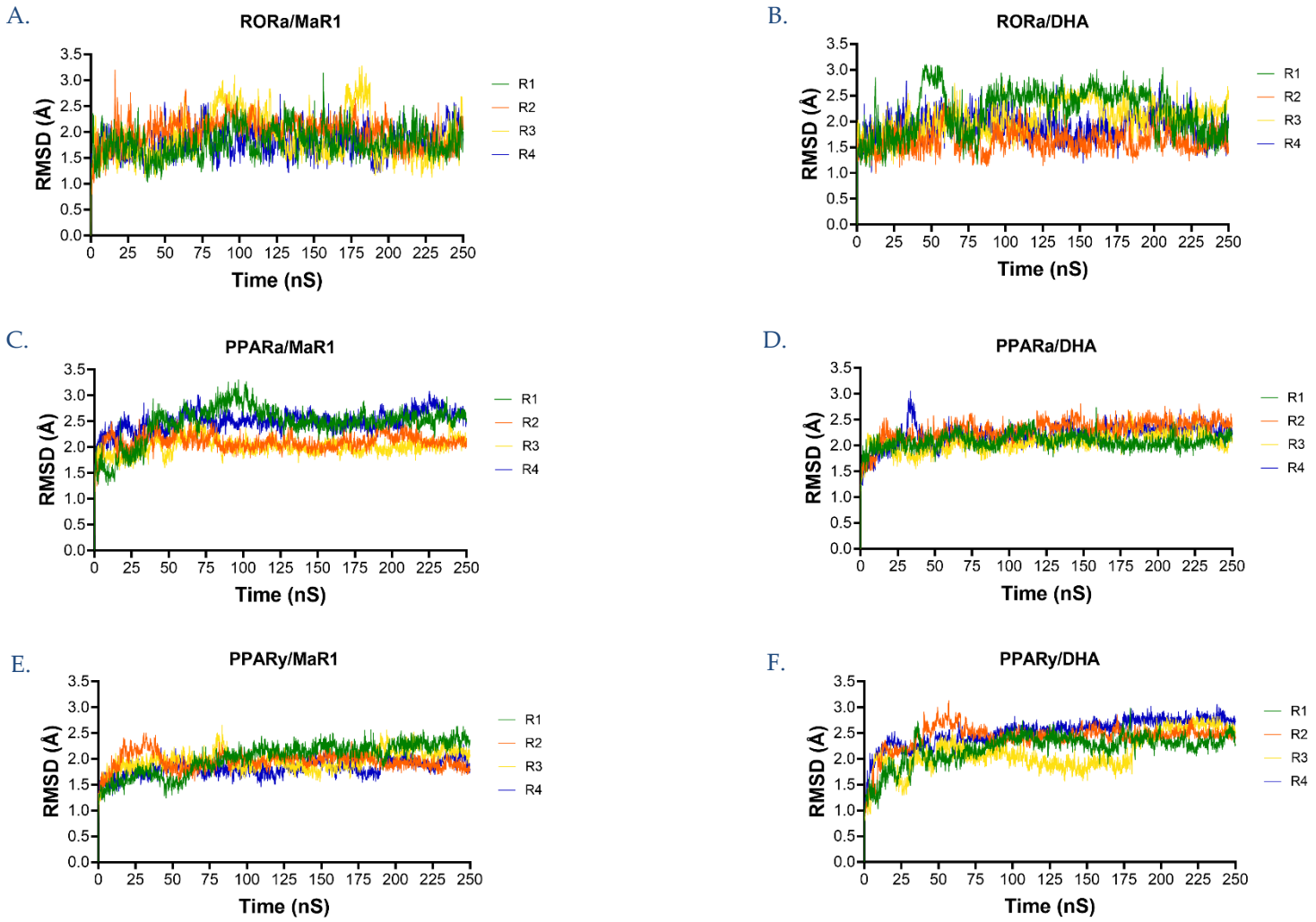


Figure S3A. Time evolution of protein backbone Cα RMSD during replicated molecular dynamics simulations of the receptor–ligand complexes. Four independent 250 ns replicas are shown for each system: (A) RORα/MaR1, (B) RORα/DHA, (C) PPARα/MaR1, (D) PPARα/DHA, (E) PPARγ/MaR1, and (F) PPARγ/DHA. We calculated RMSD values after aligning each receptor–ligand complex to its initially minimized structure.

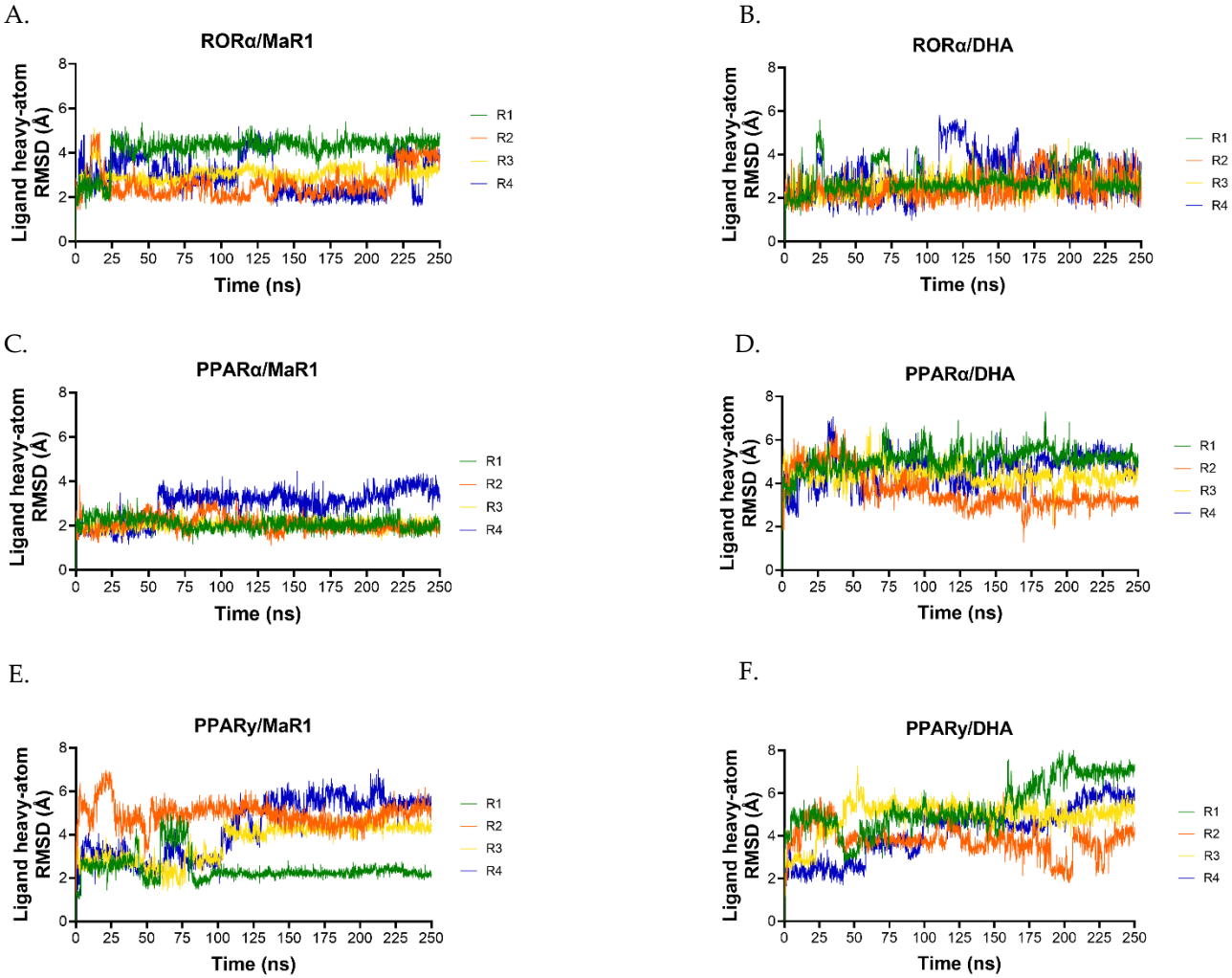


Figure S3B. Time evolution of ligand heavy-atom RMSD during replicated molecular dynamics simulations of the six receptor–ligand complexes. Four independent 250 ns replicas are shown for each system: (A) RORα/MaR1, (B) RORα/DHA, (C) PPARα/MaR1, (D) PPARα/DHA, (E) PPARγ/MaR1, and (F) PPARγ/DHA. For each trajectory frame, the receptor Cα atoms were first least-squares aligned to those of the corresponding initially minimized complex, after which ligand heavy-atom RMSD was calculated relative to the initially minimized bound pose. This procedure removes global translation and rotation of the receptor–ligand complex and describes the positional and conformational displacement of the ligand within the binding pocket. RMSD values are reported in Å. Ligand RMSD was interpreted as a structural descriptor and not as an independent measure of binding affinity.

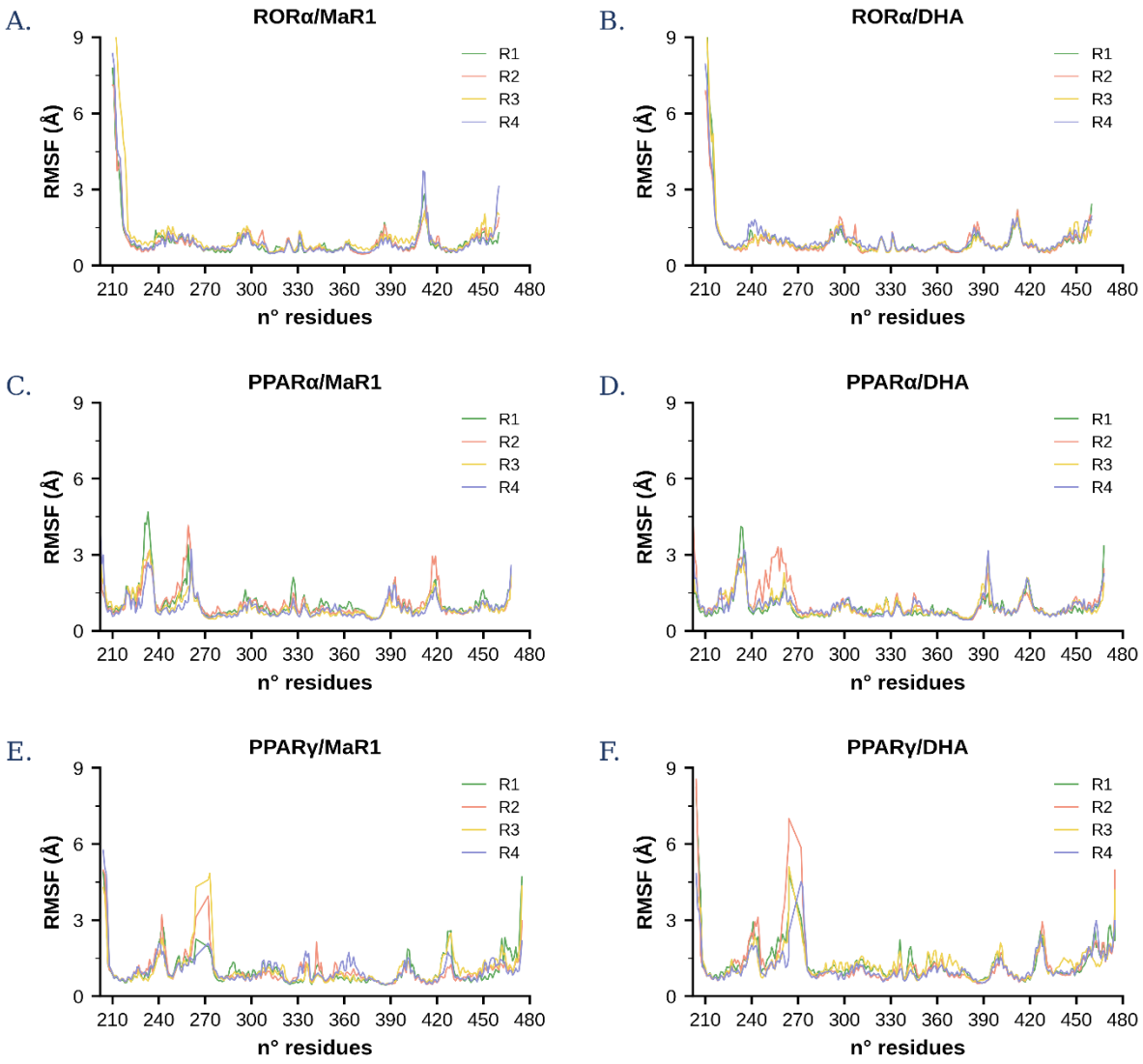
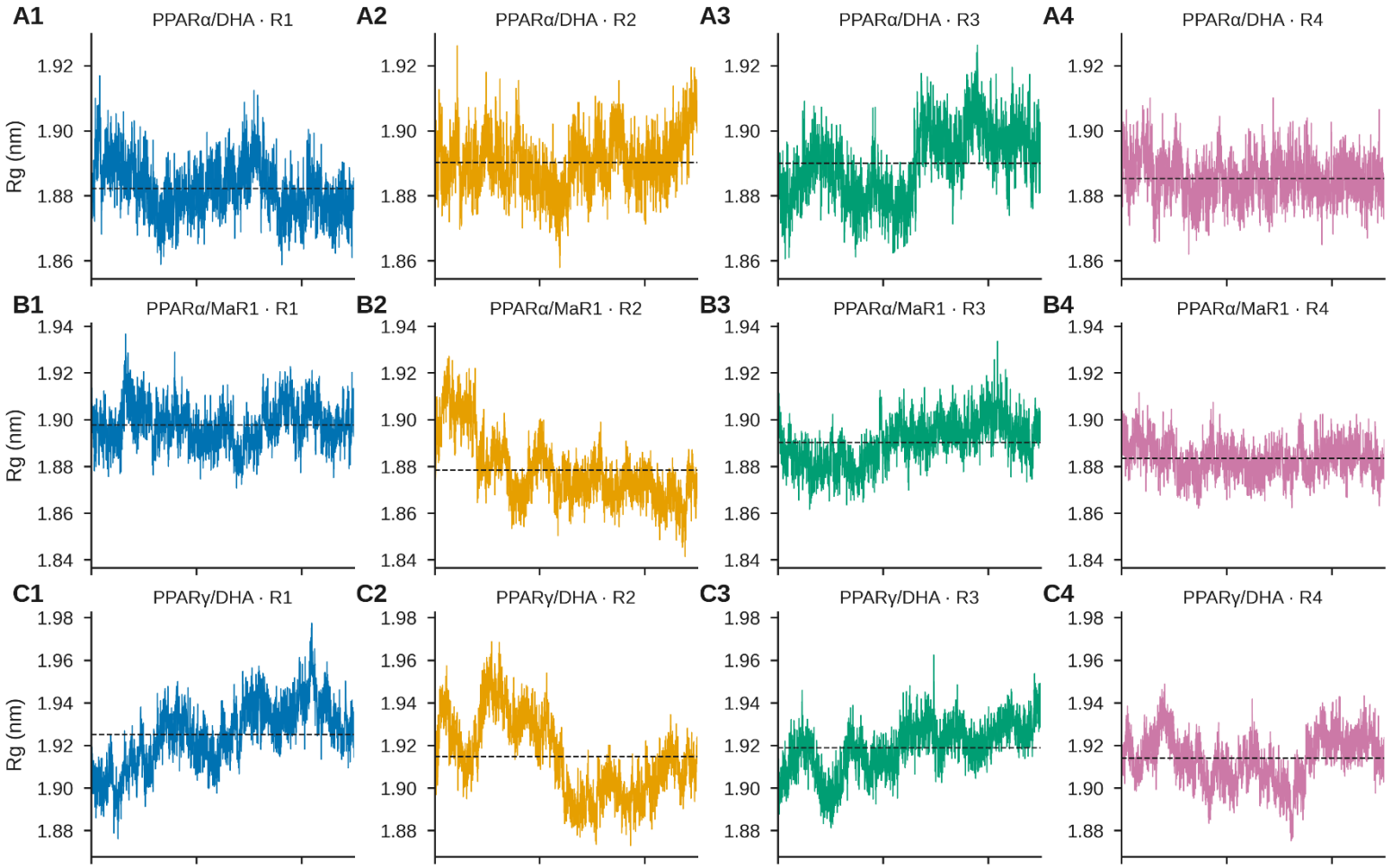


Figure S4. Per-residue Cα RMSF profiles of receptor–ligand complexes obtained from replicated 250 ns molecular dynamics simulations. Four independent replicas are shown for each system: (A) RORα/MaR1, (B) RORα/DHA, (C) PPARα/MaR1, (D) PPARα/DHA, (E) PPARγ/MaR1, and (F) PPARγ/DHA. We calculated RMSF values to assess local flexibility across the ligand-binding domains.


A1
PPARα/DHA · R1
A2
PPARα/DHA · R2
A3
PPARα/DHA · R3
A4
PPARα/DHA · R4
B1
PPARα/MaR1 · R1
B2
PPARα/MaR1 · R2
B3
PPARα/MaR1 · R3
B4
PPARα/MaR1 · R4
C1
PPARγ/DHA · R1
C2
PPARγ/DHA · R2
C3
PPARγ/DHA · R3
C4
PPARγ/DHA · R4
Rg (nm)

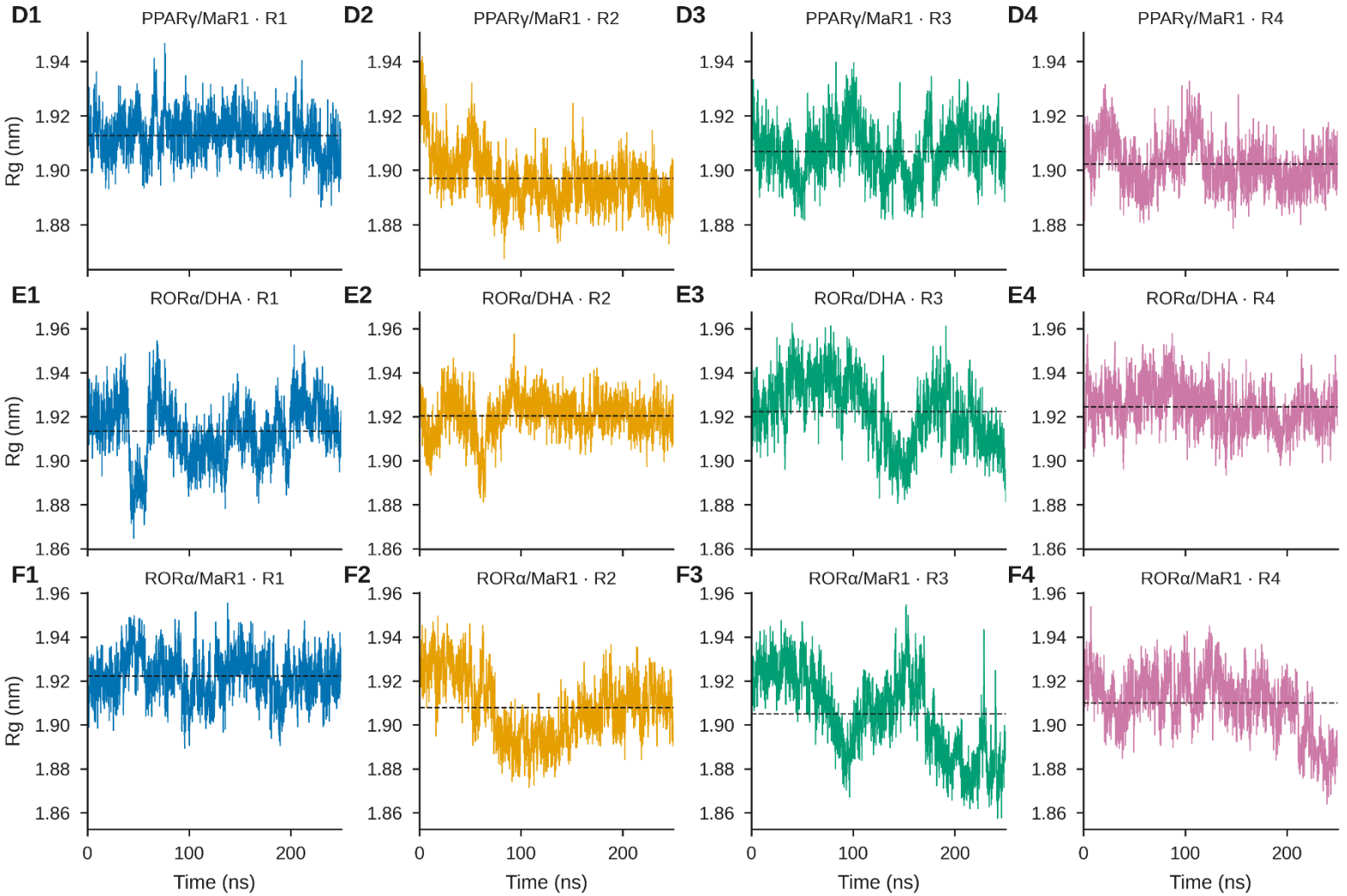
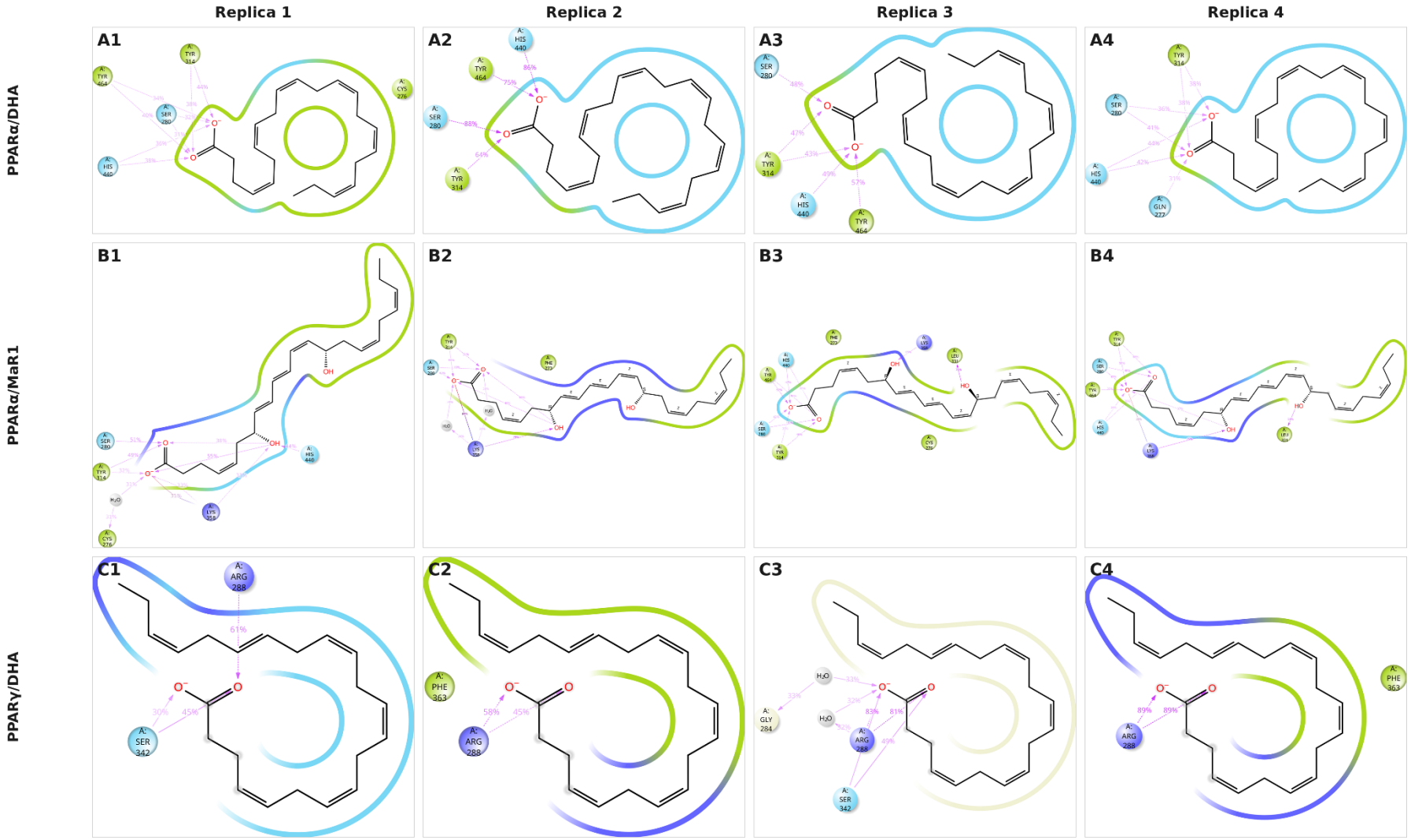


Figure S5. Per-replica radius of gyration profiles of the receptor Cα backbone during 250 ns molecular dynamics simulations of the six receptor–ligand complexes. Each panel shows one independent replica for each receptor–ligand complex: (A1–A4) PPARα/DHA, (B1–B4) PPARα/MaR1, (C1–C4) PPARγ/DHA, (D1–D4) PPARγ/MaR1, (E1–E4) RORα/DHA, and (F1–F4) RORα/MaR1. We calculated radius of gyration (Rg) values to assess the global compactness of the receptor ligand-binding domains throughout the production simulations and to support the use of Rg as one of the structural descriptors in the free-energy landscape analyses. We computed Rg using the Geo Measures Plugin for PyMOL from trajectory frames saved every 100 ps. We rendered plots in GraphPad Prism 10.6.1.


Replica 1
Replica 2
Replica 3
Replica 4
PPARα/DHA
PPARα/MaR1
PPARγ/DHA
A1
A2
A3
A4
B1
B2
B3
B4
C1
C2
C3
C4

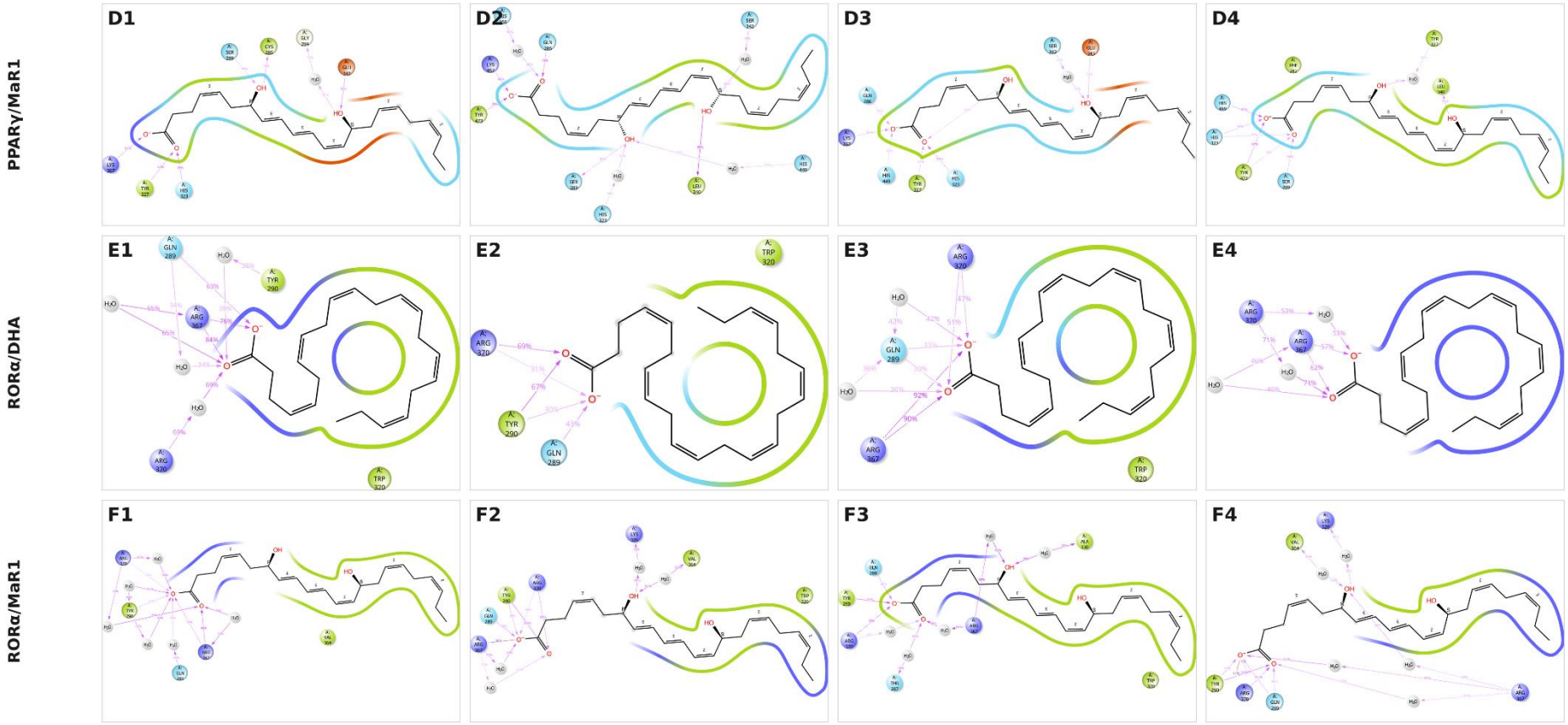


Figure S6. Replica-resolved two-dimensional protein–ligand interaction diagrams from the 250 ns molecular dynamics simulations of the six receptor–ligand complexes. Each panel summarizes the contacts detected in one independent trajectory: (A1–A4) PPARα/DHA, (B1–B4) PPARα/MaR1, (C1–C4) PPARγ/DHA, (D1–D4) PPARγ/MaR1, (E1–E4) RORα/DHA, and (F1–F4) RORα/MaR1. Hydrogen-bond, hydrophobic, ionic, and water-mediated contacts are displayed according to Schrödinger Desmond conventions. Native Desmond occupancies may exceed 100% when multiple simultaneous atom-level contacts involve the same residue. In contrast, the total per-residue occupancies in Table S8 count each residue once per frame and are capped at 100%. Principal interactions are summarized in Figure 2 and Table 4 of the main manuscript. Because these diagrams do not resolve the specific ligand oxygen group involved in every contact, oxygen-atom assignments and replica-level geometric distances are provided in Tables S9 and S10, respectively. Contact occupancies and geometric distances should therefore be interpreted as complementary descriptors.

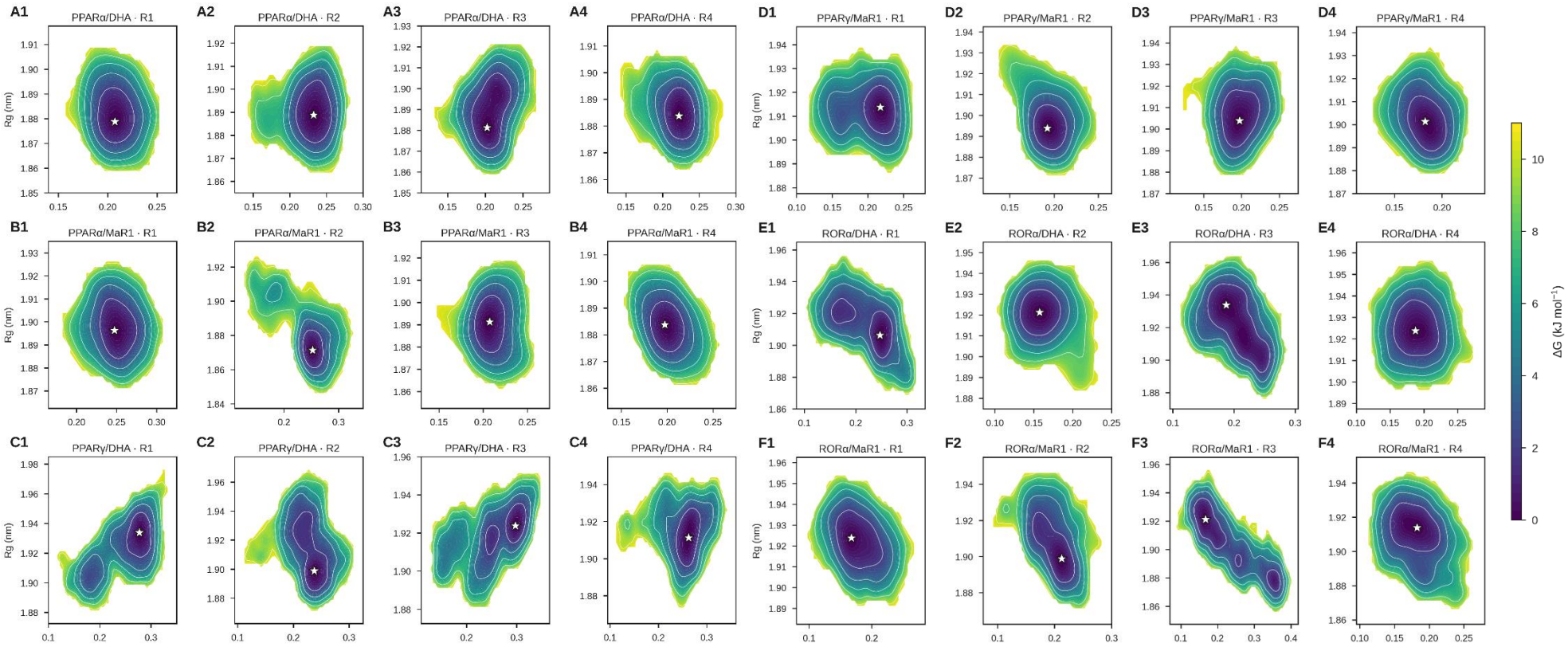
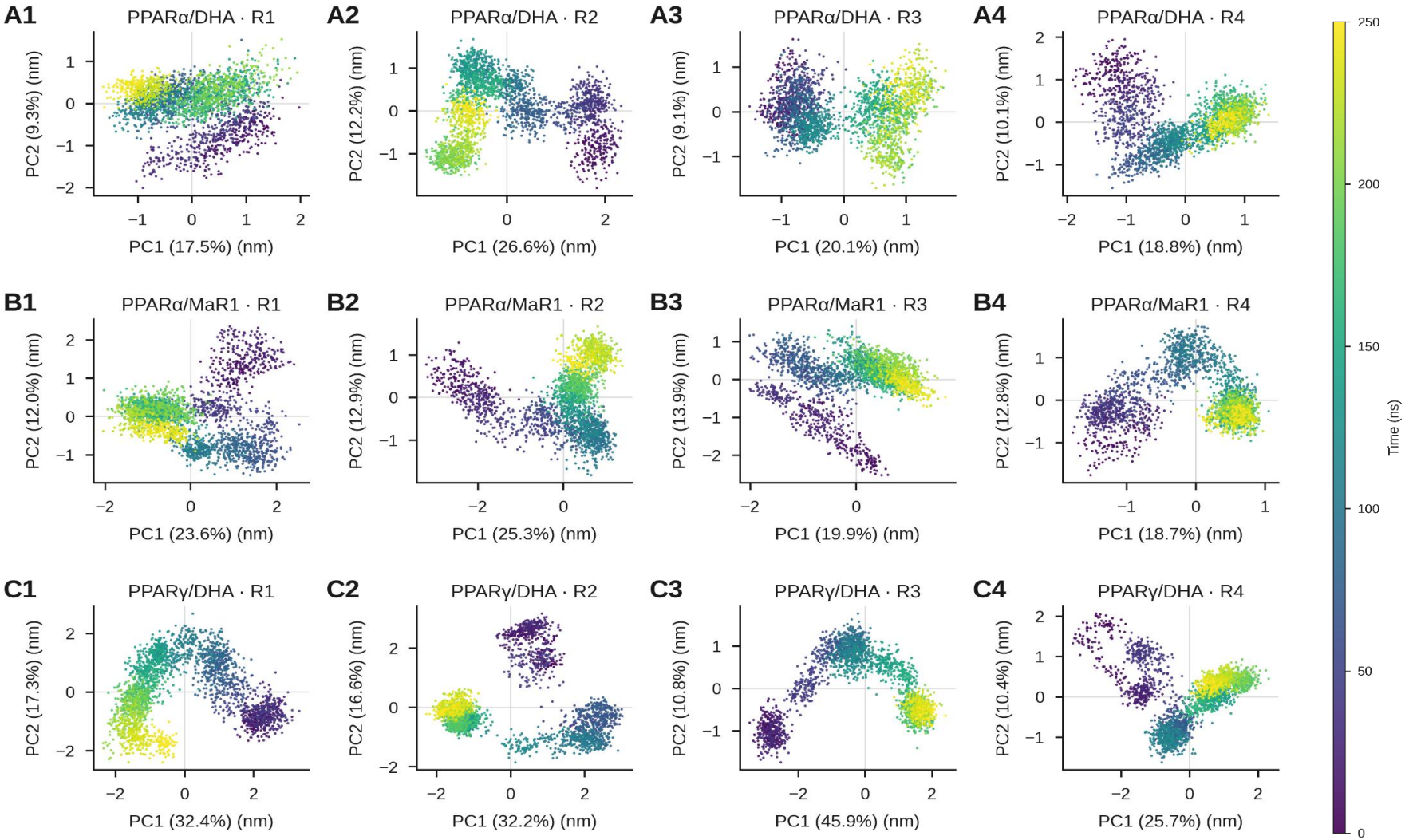
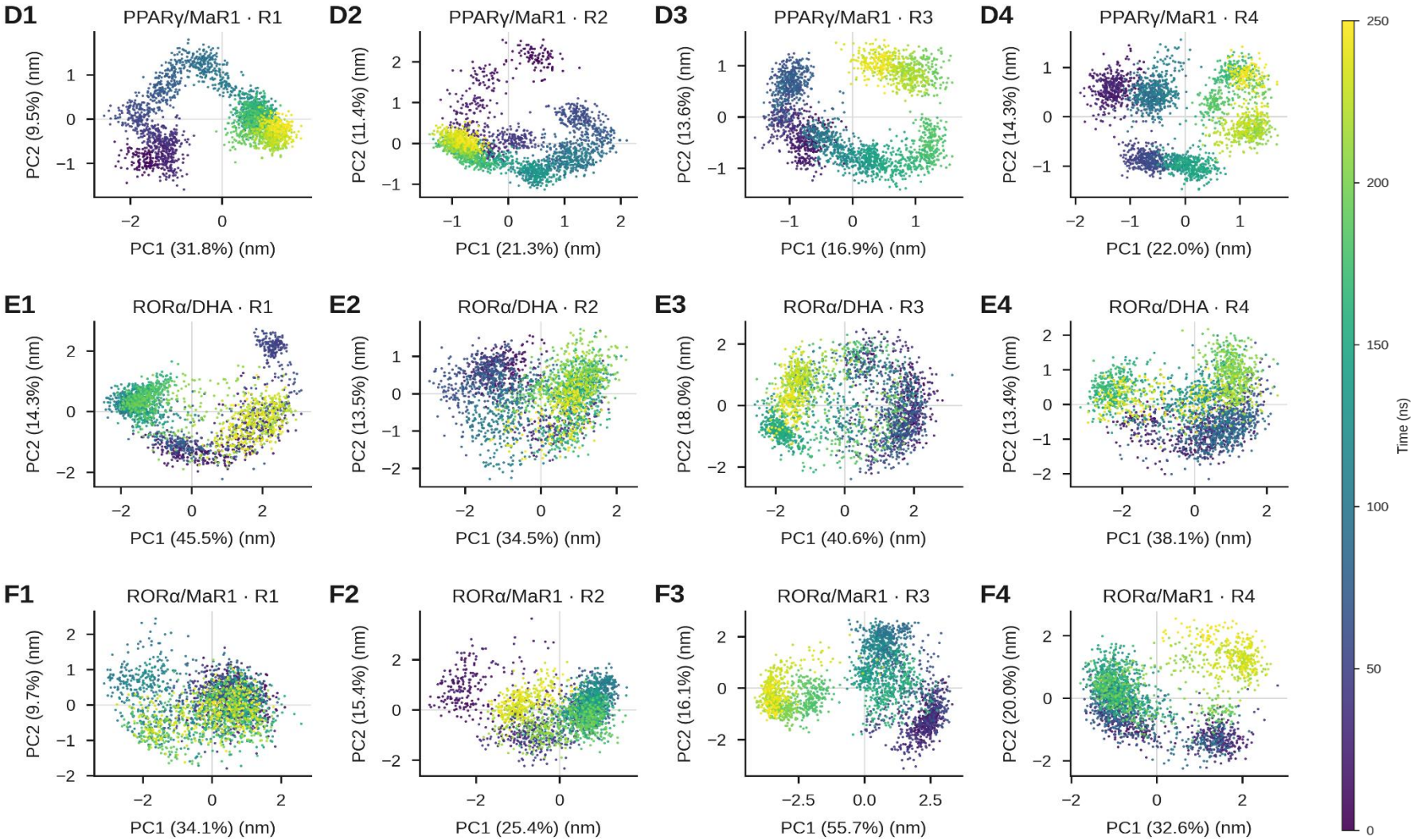


Figure S7. Replica-resolved two-dimensional apparent relative free-energy landscapes (FELs) of the six receptor–ligand complexes. Each landscape was calculated independently from 2,500 analyzed frames of one 250 ns molecular dynamics trajectory after exclusion of frame 0, using receptor Cα RMSD and protein radius of gyration (Rg) as structural descriptors. Apparent relative free energy was calculated as $\Delta G = -RT \ln[P(RMSD,Rg)/Pmax]$ at 300 K, with the global-minimum bin of each replica assigned $\Delta G = 0$ kJ·mol^{-1}. All panels use the common 0–11 kJ·mol^{-1} color scale applied in Figure 4 of the main manuscript. White stars indicate the centers of the replica-specific global-minimum bins, and white contours are drawn at 2 kJ·mol−1 intervals. Panels correspond to (A1–A4) PPARα/DHA, (B1–B4) PPARα/MaR1, (C1–C4) PPARγ/DHA, (D1–D4) PPARγ/MaR1, (E1–E4) RORα/DHA, and (F1–F4) RORα/MaR1. These replica-resolved landscapes illustrate between-trajectory heterogeneity and complement the replica-balanced pooled landscapes shown in Figure 4 of the main manuscript. Table S11 reports the numerical parameters and representative-frame identifiers of the pooled system-level landscapes and should not be interpreted as a numerical summary of the individual replica landscapes shown here.


A1
PPARα/DHA · R1
PC2 (9.3%) (nm)
PC1 (17.5%) (nm)
A2
PPARα/DHA · R2
PC2 (12.2%) (nm)
PC1 (26.6%) (nm)
A3
PPARα/DHA · R3
PC2 (9.1%) (nm)
PC1 (20.1%) (nm)
A4
PPARα/DHA · R4
PC2 (10.1%) (nm)
PC1 (18.8%) (nm)
B1
PPARα/MaR1 · R1
PC2 (12.0%) (nm)
PC1 (23.6%) (nm)
B2
PPARα/MaR1 · R2
PC2 (12.9%) (nm)
PC1 (25.3%) (nm)
B3
PPARα/MaR1 · R3
PC2 (13.9%) (nm)
PC1 (19.9%) (nm)
B4
PPARα/MaR1 · R4
PC2 (12.8%) (nm)
PC1 (18.7%) (nm)
C1
PPARγ/DHA · R1
PC2 (17.3%) (nm)
PC1 (32.4%) (nm)
C2
PPARγ/DHA · R2
PC2 (16.6%) (nm)
PC1 (32.2%) (nm)
C3
PPARγ/DHA · R3
PC2 (10.8%) (nm)
PC1 (45.9%) (nm)
C4
PPARγ/DHA · R4
PC2 (10.4%) (nm)
PC1 (25.7%) (nm)
Time (ns)
0
50
100
150
200
250


D1
PPARγ/MaR1 · R1
PC2 (9.5%) (nm)
PC1 (31.8%) (nm)
D2
PPARγ/MaR1 · R2
PC2 (11.4%) (nm)
PC1 (21.3%) (nm)
D3
PPARγ/MaR1 · R3
PC2 (13.6%) (nm)
PC1 (16.9%) (nm)
D4
PPARγ/MaR1 · R4
PC2 (14.3%) (nm)
PC1 (22.0%) (nm)
E1
RORα/DHA · R1
PC2 (14.3%) (nm)
PC1 (45.5%) (nm)
E2
RORα/DHA · R2
PC2 (13.5%) (nm)
PC1 (34.5%) (nm)
E3
RORα/DHA · R3
PC2 (18.0%) (nm)
PC1 (40.6%) (nm)
E4
RORα/DHA · R4
PC2 (13.4%) (nm)
PC1 (38.1%) (nm)
F1
RORα/MaR1 · R1
PC2 (9.7%) (nm)
PC1 (34.1%) (nm)
F2
RORα/MaR1 · R2
PC2 (15.4%) (nm)
PC1 (25.4%) (nm)
F3
RORα/MaR1 · R3
PC2 (16.1%) (nm)
PC1 (55.7%) (nm)
F4
RORα/MaR1 · R4
PC2 (20.0%) (nm)
PC1 (32.6%) (nm)
Time (ns)
0
50
100
150
200
250

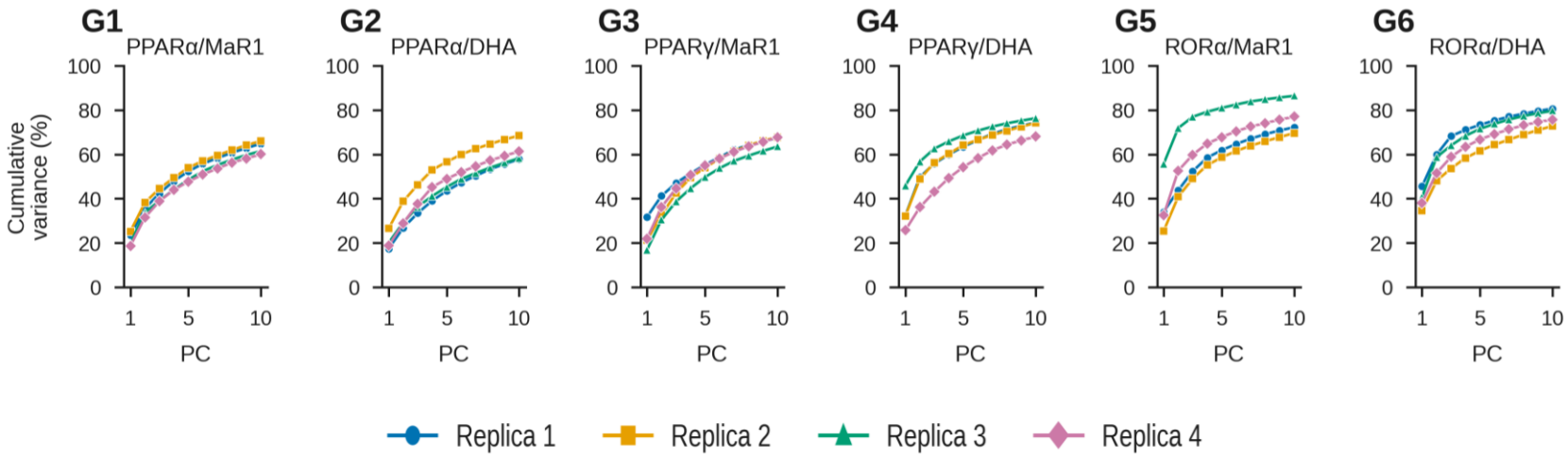


Figure S8. Replica-resolved principal component analysis (PCA) score projections and cumulative explained-variance profiles for the six receptor–ligand complexes. PCA was performed independently for each of the four 250 ns replicas per complex, corresponding to 1.0 μs of aggregate sampling per receptor–ligand system. For each replica, the receptor backbone coordinates were least-squares superimposed onto the corresponding initially minimized structure, after which a Cartesian covariance matrix of the Cα coordinates and an independent replica-specific eigenvector basis were calculated. Panels (A1–A4), (B1–B4), (C1–C4), (D1–D4), (E1–E4), and (F1–F4) correspond to PPARα/DHA, PPARα/MaR1, PPARγ/DHA, PPARγ/MaR1, RORα/DHA, and RORα/MaR1, respectively. Each point represents a simulation frame projected onto PC1 and PC2, with the color scale indicating simulation progress within the corresponding trajectory. Because an independent PCA basis was calculated for each replica, PC1 and PC2 coordinates were interpreted only within their corresponding trajectories and were not directly compared across replicas or receptor–ligand complexes. Panels (G1–G6) show the replica-level cumulative percentage of Cα backbone variance explained by the first ten Cartesian principal components for PPARα/MaR1 (G1), PPARα/DHA (G2), PPARγ/MaR1 (G3), PPARγ/DHA (G4), RORα/MaR1 (G5), and RORα/DHA (G6). Blue circles, orange squares, green triangles, and pink diamonds represent replicas 1, 2, 3, and 4, respectively. Replica-level cumulative variance and cosine-content metrics are reported in Table S12B, whereas system-level eigenvalues derived from the corresponding replica-balanced ensembles are provided in Table S12A. These projections and cumulative profiles were interpreted as descriptors of within-replica conformational sampling and not as evidence of convergence. PCA was performed using the Geo Measures Plugin for PyMOL.